A Machine Learning Framework to Identify the Correlates of Disease Severity in Acute Arbovirus Infection

Vanessa Herder[1], Marco Caporale[2], Oscar A MacLean[1], Davide Pintus[3], Xinyi Huang[1], Kyriaki Nomikou[1#], Natasha Palmalux[1], Jenna Nichols[1], Rosario Scivoli[3], Chris Boutell[1], Aislynn Taggart[1], Jay Allan[1], Haris Malik[1], Georgios Ilia[1], Quan Gu[1], Gaetano Federico Ronchi[2], Wilhelm Furnon[1], Stephan Zientara[4], Emmanuel Bréard[4], Daniela Antonucci[2], Sara Capista[2], Daniele Giansante[2], Antonio Cocco[2], Maria Teresa Mercante[2], Mauro Di Ventura[2], Ana Da Silva Filipe[1], Giantonella Puggioni[3], Noemi Sevilla[5], Meredith E. Stewart[1], Ciriaco Ligios[3], Massimo Palmarini[1*]

[1]MRC-University of Glasgow Centre for Virus Research, Glasgow, United Kingdom.

[2]Istituto Zooprofilattico Sperimentale dell' Abruzzo e Molise "G. Caporale", Teramo, Italy.

[3]Istituto Zooprofilattico Sperimentale della Sardegna, Sassari, Italy.

[4]Laboratory for Animal Health, INRAE, Ecole Nationale Vétérinaire d'Alfort, ANSES, Maisons-Alfort, France.

[5]Centro de Investigación en Sanidad Animal. Instituto Nacional de Investigación y Tecnología Agraria y Alimentaria. Consejo Superior de Investigaciones Científicas (CISA-INIA-CSIC). Valdeolmos, Madrid, Spain.

#deceased

*Corresponding author:

massimo.palmarini@glasgow.ac.uk

Abstract

Most viral diseases display a variable clinical outcome due to differences in virus strain virulence and/or individual host susceptibility to infection. Understanding the biological mechanisms differentiating a viral infection displaying severe clinical manifestations from its milder forms can provide the intellectual framework toward therapies and early prognostic markers. This is especially true in arbovirus infections, where most clinical cases are present as mild febrile illness. Here, we used a naturally occurring vector-borne viral disease of ruminants, bluetongue, as an experimental system to uncover the fundamental mechanisms of virus-host interactions resulting in distinct clinical outcomes. As with most viral diseases, clinical symptoms in bluetongue can vary dramatically. We reproduced experimentally distinct clinical forms of bluetongue infection in sheep using three bluetongue virus (BTV) strains (BTV-1_{IT2006}, BTV-1_{IT2013} and BTV-$8_{FRA2017}$). Infected animals displayed clinical signs varying from clinically unapparent, to mild and severe disease. We collected and integrated clinical, haematological, virological, and histopathological data resulting in the analyses of 332 individual parameters from each infected and uninfected control animal. We subsequently used machine learning to identify the key viral and host processes associated with disease pathogenesis. We identified five different fundamental processes affecting the severity of bluetongue: (i) virus load and replication in target organs, (ii) modulation of the host type-I IFN response, (iii) pro-inflammatory responses, (iv) vascular damage, and (v) immunosuppression. Overall, our study using an agnostic machine learning approach, can be used to prioritise the different pathogenetic mechanisms affecting the disease outcome of an arbovirus infection.

INTRODUCTION

Viral diseases are characterised by a wide spectrum of clinical symptoms that can vary substantially in their disease severity and pathogenesis. Understanding which complex virus-host interactions determine the clinical outcome of infections is the cornerstone of viral pathogenesis. Certain factors defining virus and host responses influencing disease severity are well understood[1]. For example, virus strains or variants with inherent higher or lower virulence have been described for many viruses including human or avian influenza viruses, SARS-CoV-2, dengue virus, foot and mouth disease virus, and many others[2-5]. Individual host susceptibility to virus infections is also affected by a variety of factors including age, genetic variability, pre-existing immunity, co-infections or other co-morbidities[6,7]. For example, genetic variations in genes associated with the interferon response can be responsible for more severe manifestations of acute respiratory infections such as influenza and COVID-19[8-12] . Polymorphism in chemokine receptors instead can slow progression of HIV-1 infection[13,14].

Observational studies or genome wide association studies with very large clinical cohorts are needed to correlate disease severity with distinct aspects of host responses or individual genetic differences and biomarkers[15]. These studies are feasible for diseases with a high disease burden such as COVID-19, influenza, and HIV/AIDS. However, in general, it is difficult to systematically investigate *in vivo* the fundamental aspects of the complex virus-host interactions underlying different clinical outcomes of infection. This is particularly true for many arbovirus infections, where the most common clinical outcome is febrile illness that rarely progresses to severe disease, and it is therefore mostly undiagnosed. In chikungunya virus infection for example, only a small subset of patients progress to a chronic infection and develop arthritis, which is associated with increased levels of serum cytokines and impaired immune cell functions[7]. Progressing to the severe haemorrhagic form of dengue fever virus infections is caused by the presence of anti-dengue virus antibodies from previous infections leading to a more severe disease phenotype caused by antibody-dependent enhancement[16].

Animal models are extremely useful to understand virus pathogenesis, as the various stages of disease progression can be investigated longitudinally from the very early sub-clinical incubation

period to late times post-infection. Rodent models, and the mouse in particular, have been extensively used to study viral pathogenesis. For example, gene knock-out mice have been instrumental to understand many aspects of the innate and adaptive immune response to virus infections [17,18]. However, in most cases, disease pathogenesis in experimental animal models does not fully reflect the true co-evolutionary interactions between a virus and its natural host.

In order to define the correlates of disease severity of acute arbovirus infections, we studied the pathogenesis of bluetongue, a vector-borne disease of domestic and wild ruminants. Bluetongue is caused by bluetongue virus (BTV), a dsRNA Orbivirus within the family of the *Sedoreoviridae* [19-22] transmitted by the biting midge (*Culicoides spp*). Bluetongue is endemic in most continents, and there are at least 35 BTV serotypes circulating worldwide[23,24]. BTV-8 for example, caused a major epizootic in Europe between 2006 and 2010, while BTV-3 has re-emerged very recently in the Netherlands causing major problems to animal health[25]. The re-emergence of bluetongue in Northern Europe is a stark reminder of the geographical expansion of vector-borne diseases in the last two decades[25,26].

Bluetongue is an excellent model to study the pathogenesis of acute arbovirus infections due to its wide diversity in clinical outcomes, offering a unique opportunity to dissect the intricate process governing disease severity and progression. First, the disease in sheep is characterised by a wide spectrum of clinical outcomes, ranging from a mild febrile illness to a lethal disease characterised by oedema, haemorrhages, and respiratory symptoms[27-31] . Secondly, bluetongue can be reproduced experimentally in sheep reflecting natural disease outcomes observed in the field within the same host[32,33]. Here, we aimed to investigate the complex virus-host interactions leading to different clinical trajectories in bluetongue, as a model for acute arbovirus disease. We developed an experimental framework using three different strains of BTV resulting in different clinical outcomes in sheep, ranging from clinically unapparent disease to mild and severe disease. We then used supervised machine learning[34] to evaluate more than 330 individual parameters related to virus replication and associated host responses to infection. Using this approach, we define and validate the pathways

and biomarkers associated with different clinical trajectories of disease in mammalian hosts in response to arbovirus infection.

RESULTS

Experimental reproduction of divergent clinical outcomes of bluetongue infection. To investigate the pathogenesis of acute arbovirus infection, we experimentally infected sheep with either one of the following BTV strains: BTV-1_{IT2006}, BTV-1_{IT2013}, BTV-8_{FR2017} [35,36]. We chose these three viruses as they were associated with field outbreaks of bluetongue with distinct clinical outcomes: BTV-1_{IT2006} induced severe clinical disease, BTV-8_{FR2017} caused a clinically unapparent or mild disease, while sheep infected with BTV-1_{IT2013} showed an intermediate phenotype[35,36].

We attempted as much as possible to maintain "natural" conditions in our experimental model. Therefore, we isolated these viruses directly from blood of infected animals and passaged them no more than three times in a *Culicoides* cell line to minimise mutations brought about by cell culture adaptation. We infected male and female Sarda sheep by intradermal inoculation to "mimic" an insect bite. We carried out animal experiments in two distinct locations (Table S1) using either male (location 1) or female (location 2) sheep. Henceforth, each animal experimental group will be described by "G1" or "G2" to indicate the location of the experiment, followed by the virus used for the experimental infection. For example, the group of sheep infected with BTV-1_{IT2013} in location 1 are defined as sheep "G1-BTV-1-2013". Infected animals were observed for 7 days, corresponding to the peak of clinical signs (with the exception of G1-BTV-1-2013 which were kept for 21 days). We used 7 animals for each group and included a mock-infected control group (matched for age, breed, and sex) at each location. Body temperature and clinical signs were recorded daily and compiled in clinical scores (as described in Methods and previously[37]). Although clinical scores (with the exception of fever) are predominantly based on visual examination, which can be difficult to clearly discern between intermediate phenotypes, the disease in rams in G1 typically displayed higher clinical scores, higher fever and more severe clinical manifestations than in G2. Animals G1-BTV-1-2006 displayed the most severe clinical signs; G2-BTV-8 showed the mildest outcome, while sheep

infected with BTV-1_{IT2013} showed an intermediate phenotype. Overall, we were able to reproduce experimentally the clinical outcome that was also described in the field.

Infection in sheep with BTV-1_{IT2006} was characterised by severe subcutaneous oedema (Fig. 1a) and acute respiratory symptoms with heavy breathing that presented with ulceration and erosion of the nostrils (Fig. 1b) relative to control animals (Fig. 1c), as well as severe systemic signs of infection including high fever. Female sheep infected with BTV-1_{IT2006} showed a less severe disease outcome as well lower rectal temperature compared to rams infected with BTV-1_{IT2006} (Fig. 1d-f). To confirm this apparent sex bias, we experimentally infected three additional male sheep with BTV-1_{IT2006} at location G2 (Fig. S1). In general, rectal temperatures in infected sheep peaked at 6 to 7 days post infection (dpi; Fig. 1g-h). Male sheep infected with BTV-1_{IT2006} in location G2 displayed a more severe clinical disease than female animals in the same location (Fig. S1). These data suggest that sex, not location, underlies the differences in disease severity observed in groups G1 and G2.

Male and female sheep infected with BTV-1_{IT2013} (G1-BTV-1-2013 and G2-BTV-1-2013) showed respiratory symptoms including ulceration of the nasal mucosa, nasal discharge, coughing, and a moderate subcutaneous oedema that was typically associated with increased rectal temperatures (Fig. 1g-h). Male sheep in G1 showed more severe clinical signs of infection when infected with BTV-1_{IT2006} compared to animals infected with BTV-1_{IT2013} ($p=0.0072$) at 7 dpi (Fig. 1d). However, the increase in rectal temperature of the same animals did not differ significantly at 7 dpi (Fig. 1e). Female sheep infected with BTV-$8_{FRA2017}$ (G2-BTV-8) displayed clinically unapparent or very mild clinical signs, with a minimal increase in rectal temperatures (Fig. 1g-h).

Machine learning approaches to identify correlates of disease severity. From each experimentally infected and control group we collected blood (at day 0, 1, 3, and 7 days post infection, dpi). In addition, several tissues were collected during post-mortem examination at 7 dpi (tongue, lung, skin at the site of the experimental infection, skin at a distal site of the experimental infection, and lymph nodes draining the inoculation site) from all groups with the exception of G1-BTV-1-2006. Samples were used for the following analyses: whole blood transcriptome, serum cytokines, blood biochemistry, viremia, and serology. In addition, using quantitative

immunohistochemistry of post-mortem tissues, we assessed the distribution of BTV antigens (NS2) in the tissues listed above. We also evaluated the number of follicles, and T and B cells (including Foxp3 regulatory T cells) in the lymph nodes draining the site of virus inoculation. Analysis and comparison of whole blood transcriptome between animal groups was facilitated using integrated gene sets differentiated into blood transcriptional modules (BTMs) which have been previously identified in both humans and sheep[38,39]. Hence, we collected a total of 332 parameters and established a supervised machine learning (ML) approach aimed to identify the correlates of viral pathogenesis and clinical trajectories of disease outcome.

We simultaneously analysed the data by grouping datasets in three alternative ways, according to number and type of variables: (i) 6 “states of infection”, (ii) 4 “states of infection” or (iii) “clinical states”. The “6 states of infection” analysis considered two variables, the virus strain and location/sex: G2-BTV-1-2006 (female); G1-BTV-1-2006 (male), G2-BTV-1-2013 (female), G2-BTV-8 (female) as well as control animals G1-control (male) and G2-control (female). The 7 male sheep G1-BTV-1-2013 were excluded as no post-mortem tissue from these animals could be collected at 7 dpi. The 6 “states of infection” represents the most stringent way of grouping the infected animals as they are differentiated on the bases of both the inoculated virus, sex and location of the experiment. The 4 “states of infection” analysis considered a single variable, the virus strain, irrespective of their sex or location of the experiment: G1/G2-control (male and female), G1/G2-BTV1-2006 (male and female), G2-BTV1-2013 (female only) and G2-BTV8 (female only; Fig. 2b). In the “clinical states” analysis, animals were grouped on the bases of their clinical score (irrespective of the virus used for infection) that was arbitrarily differentiated into: no clinical signs (score 0), mild disease (scores 1 to 2), moderate disease (scores 3 to 5) and severe disease (scores 6 to 8) irrespective of the virus, location or sex of the experimentally infected sheep.

We then utilised the random forest machine learning approach to analyse the data arranged in each of the groupings described above. We used recursive feature elimination to find the most predictive core subset of parameters distinguishing each group. We selected the number of parameters based on where the slope of the prediction accuracy curve plateaued, indicative of redundancy of additional

parameters (Fig. 2 a-c; Tables 1 to 3). To accurately predict the six states of infection we required a minimum of 50 out of the 332 predictive parameters, which we prioritised based on their "gini-importance" value (Fig. 2a; Table S2). This value is obtained from the sum of the number of sample splits across all decision "trees" that include the feature, proportional to the number of samples it splits[40]. Hence, this gini-importance value represents the relative importance of each parameter for classification in the random forest.

We used 1000 rounds of cross validation, each using randomly selected 5 animals from each class to train the model and 2 unseen animals to test the performance of the model. With this approach, four of six infectious states (G2-BTV-1-2006, G2-BTV-8, G1-BTV-1-2006 and G2-control) were identified with > 98% accuracy (Table 1). Infection with G2-BTV-1-2013 was predicted correctly in 82% of the cases, while the G1-control group in 98.2% of cases. The strong sex/location signal in the data are highlighted by the complete separation of the two control groups (in the ML predictions; Table 1).

Given the strong separation of uninfected male and female controls in the two locations, we sought to find parameters which predicted the infecting strain across both male and female sheep to determine generalisable trends. We therefore applied our random forest approach to the dataset arranged in the four states of infection (Fig. 2b). We found that the four groupings were accurately predicted using only 17 of the 332 parameters (Fig. 2b; Tables 2 and S3). The highest accuracy was reached with the control sheep (987/1000) containing in this instance both male and female animals from both study sites. Animals G2-BTV-8 were predicted correctly in 94.5% of the times. The most severe clinical phenotype G1-G2-BTV1-2006 was detected accurately in more than 89.9% of the time (899/1000). The lowest accuracy was evident for sheep infected with G2-BTV-1 2013 (874/1000) with overlap into other virus-infected groups (Table 2).

We then applied the same approach to the "clinical states" of infection, where animals were divided simply on the bases of the symptomatology displayed (no symptoms, mild, moderate, and severe as recorded by the clinical scores) irrespective of the virus used for the experimental infections and/or sex. The most accurate prediction was reached with 100 predictive parameters (Fig. 2c). We

obtained relatively high prediction values within the control groups (851/1000) and animals with severe disease (825/1000; Tables 3 and S4). As expected, we found lower prediction accuracy on the groups with a relatively mild or intermediate disease phenotype, as they are understandably difficult to separate on the bases of observational scores only. The low clinical score (0 to 2) was predicted correctly in 479/1000 tests while the moderate clinical scores in 694/1000, with the latter showing substantial overlaps into the groups with mild and high scores, as well as non-infected control animals. To confirm our ML results were robust and not due to overfitting on background noise, we trained random forests on shuffled data tables, where each sample's data was randomly re-assigned, removing the link between infection state, and collected data. The prediction accuracy on this shuffled dataset was lost, demonstrating the robust nature of our methodology, picking out genuine signals from the data rather than simply over-fitting (Tables S5, S6 and S7).

Key processes distinguishing the clinical trajectory of bluetongue. We next focused our study on those parameters with the highest gini-importance values that were common predictors for at least two of the three groupings described above. This unbiased approach identified in total 35 parameters (Fig. 3 and Table S8), and among these, 8 (Fig. 3a, arrows) were shared by all 3 approaches. Overall, from these parameters, we identified five different fundamental processes in virus-host interactions affecting the clinical trajectory of bluetongue: (i) virus load, (ii) the host type-I interferon (IFN) response; (iii) pro-inflammatory responses, (iv) vascular damage, and (v) immunosuppression (Fig. 3b-c).

Virus load and replication in target organs. Blood viremia, assessed as the amount of viral RNA in the blood, was the parameter with the highest impact on the severity of the disease identified by our machine learning approach (Fig. 3a). We detected viral RNA in the blood of some infected animals from 1 dpi. By 3 dpi most infected animals, except G2-BTV-8 tested positive for viral RNA. All animals, with the exception of 4 BTV-8 infected sheep and the control groups, became viraemic at 7 dpi (Fig. 3c, 4a). Importantly, we detected the highest values of viral RNA at 7 dpi in the blood in those G1-BTV1-2006 animals with the most severe clinical symptoms, highlighting a positive correlation between viremia and severity of clinical signs (Fig 4a).

The relative amount of virus antigen in the tissues of infected animals at 7 dpi was also one of the 35 key parameters distinguishing clinical outcome (Fig. 3b). We assessed BTV replication in the tissues of infected animals by quantifying NS2-positive signal by immunohistochemistry. We applied software-assisted unbiased image analysis on stained tissue from tongue, lung, skin (both at the sites of virus inoculation and in a distant site), and in the lymph nodes draining the site of inoculation. In general, tongue and lung from BTV-infected animals showed the highest relative values of viral protein expression (Fig. 4b-h). Impairment of these organs is consistent with the dominant clinical symptoms of bluetongue in sheep including lesions to the tongue and respiratory distress. We detected BTV antigen and RNA in the endothelial cells of the tongue by both immunohistochemistry and RNA *in situ* hybridisation, respectively (Fig. 4c-h). The skin of animals with bluetongue also showed erythema. In the lung, bronchial and alveolar epithelial cells were positive for viral antigen. At 7 dpi in the BTV-infected animals, G1-BTV-1-2016 demonstrated the highest proportion virus-infected cells than sheep in groups G2-BTV-1-2013 and G2-BTV-8 (Fig 4b). We found virus in the endothelial cells of small blood vessels of both the skin corresponding to the sites of virus inoculation, and in distant areas. These data suggest that the virus infects the endothelial cells of the deep dermis after the viraemic phase. However, confocal microscope analysis of additional skin samples at the site of virus inoculation, collected at earlier time points (2 dpi) from animals infected with BTV-1_{IT2006} (included in a separate pilot experiment), showed BTV to mainly infect the endothelial cells of the lymphatic vessels (Fig. 4i).

Overall, these data show that the severity of disease is correlated to BTV infection of endothelial cells in peripheral organs including skin, lungs, and tongue which are reached by the virus during the viraemic phase of disease progression.

Timing of the type-I IFN response. The second parameter with the highest gini-importance value, among the 35 identified above (Fig. 3a), were BTMs which included genes involved in the type-I interferon (IFN) response (BTM M68 and others; Table S8). These BTMs include transcription factors such as IRF-7 and interferon stimulated genes like CXCL10, ISG15, IFIT-1, IFIT-2, RSAD2, OAS1 among others. Other BTMs highlighting innate immune activation include those associated with

dendritic cell activation (BTM M67), and general chemokine, inflammatory and innate activation (BTMs M13 and M86.0). Importantly, analysis of blood transcriptome using standard pathway analysis methods also revealed “cytokine signalling in immune system” (GO:0019221), “innate immune responses” (GO:0002226) and “interferon signalling” (GO:0060337) as the strongest upregulated pathways discriminating the different clinical outcomes of bluetongue infection (Fig. S2).

Overall, the data described above indicate that the type-I IFN response is a key correlate of disease outcome. Hence, we further analysed the transcriptional profile of interferon stimulated genes, which collectively orchestrate the host antiviral state, in the blood of infected and uninfected animals from the early phase of the infection, to the peak of clinical manifestations (1 to 7 dpi, respectively) to capture the temporal modulation of the IFN response. Animals infected with BTV-8 (which presented a very mild to asymptomatic infection) showed the strongest early upregulation of ISGs (1 dpi; Fig. 5a). Indeed, it is notable that we could detect upregulated BTMs associated with innate immune response (and pro-inflammatory response – see below) in all animals infected with BTV-8_{FR2017}, although viremia was only detected in 3 of the 7 infected sheep.

Conversely, sheep within the G1-BTV-1-2006 group, with the severe clinical phenotype, showed instead no upregulated ISGs at 1 dpi (Fig. 5a), while animals infected with BTV-1_{IT2013} with an intermediate phenotype showed mild upregulation of ISGs. At 3 and 7 dpi instead, sheep within the groups with most severe disease (G1-BTV-1-2006) showed the strongest ISG induction, while it was minimal in G2-BTV-8 animals. These data suggest that replication of the less virulent virus BTV-8_{FR2017} was controlled by the host type-I IFN response at the early stages post-infection, while the more virulent BTV1_{IT2006} was able to block the early IFN response *in vivo*.

To corroborate these data, we infected ovine endothelial cells with the viruses used in this study and analysed the ISG response at 6 and 12 hpi *in vitro*. Similarly, to what we observed *in vivo,* at early times post-infection, BTV-1_{IT2006} induced a relatively reduced ISG response compared to BTV-8 (Fig. 5b). These data suggest that the most virulent virus, BTV-1_{IT2006}, is better equipped to modulate the IFN response compared to the BTV-8_{FR2017}.

289 **Pro-inflammatory response leading to vascular damage.** The next three parameters with the
290 highest gini-importance values were all related to the host pro-inflammatory response. BTM 86.1
291 was the parameter with the third highest gini-importance value, and included many proinflammatory
292 mediators such as IFNɣ, TNF, CCL4, CCL20 and NFKB1. This BTM was more strongly upregulated
293 in sheep with more severe disease compared to those in the G2-BTV-8 group and the mock-infected
294 controls. Importantly, these data extracted from RNAseq, were confirmed by Luminex© assays
295 highlighting a significant upregulation of cytokines including IFN-ɣ and CXCL10/IP-10 (fourth and
296 fifth highest gini-importance values) in the sera of sheep with more severe and moderately serious
297 clinical signs, compared to groups with milder disease (Fig. 6a). Other BTMs among the 35 key
298 predictive parameters of disease severity included M13 and M86.1 that overlap with M86.1 above
299 and genes associated with the innate immune response and proinflammatory mediators such as
300 IL1β. Overall, data obtained from both RNAseq and Luminex assays demonstrate disease severity
301 is to be tightly associated with the induction of pro-inflammatory cytokines.

302 The presence of pro-inflammatory mediators in the blood can contribute to vascular damage.
303 Correspondingly, the sixth predictive parameter of BTV disease severity was the amount of total
304 blood proteins detected in infected animals. Animals with severe bluetongue showed a profound loss
305 of total proteins in the blood, which is a consequence of vascular damage (Fig. 6b). Furthermore,
306 genes associated with platelet activation (BTM M196) were also strongly upregulated in severe
307 cases of bluetongue (G1-BTV-1-2006). Furthermore, RNAseq pathway analysis also confirmed
308 genes associated with vascular disease to be more significantly upregulated in severely ill sheep
309 (Fig. S2c).

310 **Immunosuppression.** The next parameter with the highest gini-importance values was BTM S8,
311 which is associated with naïve B cell surface signatures. Importantly these were reduced in sheep
312 with more severe disease. Notably, two other BTMs associated B-cell enrichment (BTM M47.3 and
313 BTM M47.4) were also identified in the top 35 parameters suggesting a trend in B cell reduction in
314 animals with severe disease. These data are in line with previously published reports showing that
315 BTV causes lymphopenia[41] and a transitory immunosuppression due to inhibition of B-cell division

316 in germinal centres due to infection of follicular dendritic cells[32,42]. Indeed, we detected a reduced
317 number of follicles in the lymph nodes draining the sites of virus inoculation in animals with severe
318 disease (Fig. 6d). We also confirmed lymphopenia in G1-BTV-1-2006 animals compared to control
319 animals, although for logistic reasons we could not perform this particular experiment in animals in
320 the G2 group (Fig. 6c). Importantly, we identify BTM 7.3, associated with genes related to T-cell
321 activation, to be significantly upregulated in animals with no (G2-BTV-8) or moderate disease relative
322 to severe disease (G1-BTV-1-2006). In addition, we further analysed regulatory T cells (Treg), as
323 they are key drivers in the modulation of antiviral immunity. We detected a significant reduction of
324 $Foxp3^+$ Tregs in the lymph nodes of G1-BTV-1-2006 animals compared to $BTV\text{-}8_{FR2017}$ and BTV-
325 1_{IT2013}-infected ones at 7 dpi (Fig. 6e). The reduction of Tregs in severely diseased animals suggests
326 an important role of this T cell subgroup in the outcome of BTV pathogenesis, which are known to
327 control virus-induced tissue damage and dampen overwhelming immune responses[43,44]. Overall,
328 immunosuppression was also confirmed by RNAseq pathway analysis, which demonstrated
329 significantly higher levels of differential gene expression in G1-BTV-1-2006 (Fig. S2d).

330

331 **Discussion**

332 In this study we comprehensively investigated the pathogenic mechanisms underlying the clinical
333 outcomes of arbovirus infection. Arboviruses are the cause of major global health and economic
334 burden[45]. While each arbovirus has its own distinctive clinical features, many of these vector-borne
335 diseases in humans (and animals) are typically characterised by general symptoms such as mild
336 febrile flu-like illness and rash, with only a minor proportion of cases exhibiting severe clinical
337 manifestations[46,47]. It is therefore critical to understand the underlying biological processes
338 responsible for the varied pathogenic outcomes to arbovirus infection and their relative importance
339 to disease outcome in a systematic manner.

340 In this study, we used bluetongue, a major vector-borne disease of ruminants, as an experimental
341 model in its natural host species. We were able to experimentally recapitulate the varied clinical

342 outcomes of BTV infection in sheep, ranging from unapparent or mild febrile symptoms (BTV-8_{FR2017})
343 to more severe disease (BTV-1_{IT2006}), including respiratory distress, sub-cutaneous haemorrhage,
344 oedema, and tongue lesions. We collected data encompassing 332 biological parameters related to
345 both virus and host from infected or control animals, and used machine learning to prioritise the key
346 correlates of disease severity.

347 Machine learning is being increasingly used in the infectious disease field to find applicable
348 biomarkers of disease trajectories [48-50]. In most cases, however, this approach relies on disease
349 systems trained on data obtained from large patients cohorts or previously characterised patients[34].
350 Here, we used machine learning in an unbiased approach to identify the key drivers of the
351 pathogenesis of an arbovirus infection. Our approach identified the (i) levels of virus replication in
352 the infected host, (ii) timing of the host innate immune response, (iii) levels of pro-inflammatory
353 mediators, (iv) vascular damage, (v) and immunosuppression to be critical in contributing functions
354 of disease progression and severity (Fig. 7).

355 Viral load in the blood was the highest parameter that directly correlated to disease severity. Levels
356 of viremia were related to the detection of virus in endothelial cells in the lung, tongue, and skin of
357 infected sheep, which directly recapitulate the clinical signature of bluetongue: respiratory distress,
358 lesions in the tongue epithelium, and sub-cutaneous haemorrhage.

359 The second prioritised parameter by our experimental approach was related to the type-I IFN
360 response, one of the key host antiviral innate immune responses. Resolving viral infection in
361 mammals is associated with an effective “antiviral state”, which is orchestrated by the production of
362 interferons inducing the activation of hundreds of interferon-stimulated genes (ISGs)[51]. At 7 dpi (peak
363 clinical symptoms), a stronger systemic IFN response correlated with more severe disease.
364 However, at early time points (1 dpi) there was an inverse correlation. We detected a stronger
365 systemic type-I IFN response in sheep infected with the attenuated BTV-8_{FR2017} (G2-BTV-8 group)
366 compared to those with a more severe disease. This trend was confirmed *in vitro*, where cells
367 infected with BTV-1_{IT2006} showed reduced ISG expression at 6 hpi compared to cells infected with
368 BTV-8_{FR2017}. We conclude that more virulent BTV strains appear to be efficient at modulating the

type-I IFN response, allowing the virus to reach higher viral loads and further dissemination to target organs. These data are consistent with our recent findings in BTV infected primary bovine cells[52]. Cows are known reservoirs of BTV infection but rarely show clinical disease. Comparison of a virulent strain of BTV in ovine and bovine cells identified the type-I IFN response to be initiated earlier in bovine cells leading to a greater restriction in virus replication[52]. BTV modulates the interferon response through the expression of non-structural proteins with immunomodulatory functions, such as NS3 and NS4, and by inducing host cell translational shutdown[53-57]. It is most likely that BTV strain- and/or species-specific variance in the expression and/or biological activity of these viral immune evasion agonists account for the differences observed in type-I IFN response.

In addition, we found a high pro-inflammatory immune signature to correlate with disease severity. We identify both the transcript levels of inflammatory genes and pro-inflammatory cytokine mediators (IFN-γ and CXCL-10/IP-10) to strongly correlate with disease progression. CXCL10/IP-10 expression has been shown to be induced by IFN-γ in a range of cell types, including leukocytes, neutrophils, eosinophils, endothelial cells, and monocytes, and to correlated with disease severity[58]. Virus replication in endothelial cells, but more importantly a systemic pro-inflammatory immune response can contribute to increased capillary permeability, vascular leakage and therefore loss of blood protein in interstitial spaces. Indeed we found that the reduction of total blood proteins (proteinemia) in infected animals to be directly related to disease severity. Vascular damage and hypoproteinaemia lead to haemoconcentration, based on reduced oncotic pressure, and oedema, which is one of the key symptoms that we detected in sheep with more severe clinical disease (Fig. 1). Vascular leakage is also a pathological feature severe of dengue virus infection[59].

Like many acute infections, BTV is initially controlled by the type-I IFN response prior to induction of the adaptive immunity. We did not systematically characterise the host adaptive immune response in this study, but we could detect (i) a reduction of B-cell signatures in the blood transcriptome, and (ii) a reduction in the number of B-cell follicles in the regional lymph nodes draining the sites of virus inoculation in sheep affected by more severe disease. These data support previously published studies identifying peripheral B-cell reduction in BTV-infected animals[60], and demonstrating BTV

disruption of follicular dendritic cells the in regional lymph nodes close to the site of inoculation, leading to a block in B-cell maturation and immunosuppression[61]. In addition, animals within the G1-BTV-1-2006 group showed a marked leukopenia (compared to G1-control and G1-BTV-1-2013), which is a common feature in BTV-infected animals[62]. Overpowering immune responses and virus elimination are controlled by regulatory T cells (Tregs)[63]. Tregs during virus infection limit the efficiency of anti-viral immunity and tissue damage due to excessive inflammation. Here, we identify a severe disease phenotype of BTV infection in sheep to substantially reduced Treg-numbers in the draining lymph nodes. These data suggest that a prolonged impairment of Tregs during acute BTV-infection may have a substantial negative impact upon the outcome of the disease, as previously described for other infections[64,65-67].

In summary, our systematic experimental approach, and the use of machine learning, has identified the key parameters of an arboviral disease progression. We showed how bluetongue disease severity is directly linked to immunopathology, which in turn is governed by the balance between virus replication, and the host innate and adaptive immune responses. Early activation of the type-I IFN response strongly correlates to reduced viral load, reduced pro-inflammatory responses, and a milder clinical outcome of infection. On the other hand, late IFN responses are instead associated with high viral load, high pro-inflammatory responses, vascular damage, and immunosuppression leading to more severe disease outcomes (Fig. 7). Our study provides an overall framework to understand and compare the pathogenesis and disease progression of arbovirus infections.

Materials and methods.

Cells and viruses. The three viruses used in this study, BTV-1_{IT2006}, BTV-1_{IT2013} and BTV-8_{FR2017} originated from blood of infected sheep[35,36] and were isolated and passaged up to three times in KC cells[68]. These cells are derived from *Culicoides sonorensis*, and were grown at 28°C using Schneider's insect media (Sigma-Aldrich) with 10% foetal calf serum (FCS; ThermoFisher). Supernatants were harvested 5 days post infection (dpi) and virus titres determined by standard plaque assays in CPT-Tert cells as previously described[69,70]. As a control, supernatant of non-

423 infected KC cells diluted with PBS was used. CPT-Tert cells[71] derive from sheep choroid plexus cells
424 immortalized with simian virus 40 (SV40) T antigen and human telomerase reverse transcriptase,
425 and were propagated in Iscove's modified Dulbecco's medium (IMDM) supplemented with 10% FBS.
426 Immortalised primary ovine endothelial cells were used as described previously[52]. For the RNAseq
427 experiments described below, immortalised ovine endothelial cells were infected in 12-well plates at
428 MOI~10 with either BTV-1_{IT2006}, BTV-1_{IT2013} or BTV-8_{FR2017} by spinoculation at 500 x g at 4°C for 1 h.
429 The inoculum was aspirated, cells washed twice with warm media supplemented with 10% FCS and
430 incubation at 37°C in a humidified 5% CO2 environment for either 6 or 12 hpi. After incubation,
431 monolayers were washed with warm PBS to remove any cellular debris and immediately lysed in
432 750 µL of Trizol. Total RNA was extracted from each sample as previously published [52].

433 **Animals and study design.** All animal experiments described in this study were approved by the
434 local committees of the Istituto Zooprofilattico Sperimentale dell'Abruzzo e del Molise "G. Caporale"
435 (Teramo, Italy) and Istituto Zooprofilattico Sperimentale della Sardegna (Sassari, Italy) and further
436 approved from the Italian Ministry of Health in accordance with EU laws 26/2014 (permission
437 numbers 797/2018-PR and 688/2018-PR). Sarda sheep were kept in mosquito-proof, air-controlled
438 facilities with *ad libitum* access to tap water to acclimatise before being enrolled in the experiments.
439 Animals were fed pellets and hay daily. 59 adult sheep (Sarda breed) were infected with BTV-1_{IT2006},
440 BTV-1_{IT2013}, BTV-8_{FR2017} or mock-infected, respectively (Table S1). Experiments were carried out in
441 two distinct locations (G1 and G2). Rams were used in location G1, while ewes in location G2. In the
442 location G1, in total 21 male Sarde sheep were inoculated (mock, BTV-1_{IT2006}, BTV-1_{IT2013}, n=7,
443 respectively). Sheep with mock and BTV-1_{IT2013} were sacrificed at 21dpi, while BTV-1_{IT2006} animals
444 were culled between 7 and 9 dpi due to welfare reasons. In the location G2, in total 28 female sheep
445 (mock, BTV-1_{IT2006}, BTV-1_{IT2013}, BTV-8_{FR2017}; n=7 per group) were kept for 7 dpi. Two additional
446 experiments were carried out in location G2: 3 male sheep were infected with BTV-1_{IT2006} in location
447 G2 and culled at 7 dpi. In addition, 4 female sheep were infected with BTV-1IT2006, or mock-
448 infected, and killed at two days post-infection (Table S1).

Each animal was inoculated intradermally with multi-site injection in 4 distinct areas (500µl per inoculation area) in proximity of the right axillary, left axillary, right inguinal and left inguinal lymph nodes. In total, we used $2x10^5$ pfu of virus per animal. Control animals received the same treatment with the same volume of diluted, mock-infected Kc cell culture supernatant. Animals were killed at 7 dpi, with the exception of 4 animals infected with BTV-1_{IT2006} in location G1 which were killed at 8 or 9 dpi. As highlighted above, three additional rams were used in location G2 to control for sex differences in the severity of BTV-1_{IT2006} infection. In addition, to control for the early sites of viral replication in the skin, 4 ewes and mock-infected controls were killed at 2 dpi. Animals used in the experiment were screened for the presence of antibodies towards BTV [72] and for viral RNA in the blood by qRT-PCR (see below). Only seronegative and PCR negative animals were used in the study. Animals were dewormed with netobimin 4ml/10kg body weight. Blood for haematology was collected only from animals in location G1. Sera were instead collected for serology, blood chemistry and cytokines analysis (from both animals in G1 and G2). For RNAseq, 2.5ml blood from animals in G1 and G2 was collected in PAXgene Blood RNA Tubes (IVD, Qiagen, 762165). Rectal temperature and clinical score were assessed by 2 veterinarians daily according to the previously published scoring index[37]. Tissues samples were collected at post-mortem and fixed in 4% buffered formalin (FFPE), or PAXgene fixative (PFPE, PAXgene Tissue FIX Container; 50 ml; Qiagen, 765312), for 16 hours and subsequently embedded in paraffin wax. All paraffin wax embedded tissue blocks were stored at 4°C until use.

Serology. The presence of anti-VP7 BTV antibodies in UV-light inactivated serum was investigated using the ID Screen Bluetongue Milk indirect kit (ID vet, Innovative Diagnostics; BTSMILK-4P) according to manufacturer's protocol. Sheep sera were diluted from 1:20 to 1:2560 and samples were tested in two technical replicates. Serum samples were tested on day 0 and 7 post infection. A BMG Labtech PHERAstar *FS* Elisa plate reader was used to obtain the data.

Blood biochemistry and haematology. The blood was collected in vacuum tubes without anticoagulant for biochemical analysis, left at room temperature to allow clot retraction, and then centrifuged at 2000g for 4 minutes. Samples were analysed using the ILAB 650 automated system

(Instrumentation Laboratory-Werfen, MA, USA) with the Quantilab Kits (Werfen Company, Milan, Italy) according to manufacturer's instructions. For the haematological analyses, tubes containing ethylenediaminetetraacetic acid (EDTA) at 4°C were analysed within 24 h after collection. Samples were analysed with an ADVIA 120 haematology system (Siemens), equipped with specific software for veterinary use.

Cytokines. To levels of cytokines in the sera of infected animals were obtained using the MILLIPLEX® MAP Bovine Cytokine/Chemokine Magnetic Bead Panel 1 - Immunology Multiplex Assay Kit (Merck-Millipore, BCYT1-33K) and the Bovine IFN-alpha ELISA Kit (Sigma-Aldrich, RAB1012) according to the manufacturer's instructions. Sera were diluted 1:2 and UV-inactivated before use.

RNAseq. Two RNAseq analyses were carried out in this study on (i) RNA extracted from blood of infected and mock-infected animals (G1 and G2) at 1, 3 and 7dpi, and (ii) RNA extracted from immortalised ovine endothelial cells infected (or mock-infected) at 6, and 12 hpi**.** RNA from blood samples was isolated using the PAXgene Blood RNA Kit (Qiagen, 762164) according to manufacturer's instructions. Isolated RNA was stored at -80°C until processed. RNA concentration was assessed with a Qubit Fluorimeter (Lefe Technologies) while RNA integrity was calculated using an Agilent 4200 TapeStation. RNA from blood samples had an average RNA integrity value of 8 or above. From these samples, libraries for sequencing were generated using a Lexogen QuantSeq 3' mRNA-seq (FWD) kit, according to the manufacturer's instructions. Briefly, 35ng of total RNA from each sample was taken for library preparation. cDNA was synthesised directly from the polyadenylated 3' mRNA end with an oligodT. The RNA template was then enzymatically depleted and specific globin probes, that block the processing of alpha and beta haemoglobin sequences, were added to the cDNA. The primed cDNA was then converted to dsDNA by second strand synthesis using random primers containing Unique Molecular Identifiers (UMIs). Libraries were pooled in equimolar concentrations and sequenced in Illumina NextSeq 500 and 550 sequencers using a high-output cartridge, generating single reads with a length of 75 bp. At least 91% of the reads generated presented a quality score of 30 or above.

RNA of infected and mock-infected immortalised ovine endothelial cells was extracted as previously described[51] and had an average RNA Integrity Number of ~9.8. 500 ng of total RNA from each sample was taken for library preparation using an Illumina Stranded Total RNA Prep Ligation with Ribo-Zero Plus, according to the manufacturer's instructions. RNA was depleted of ribosomal RNA using specific probes and then fragmented. RNA fragments were reverse transcribed and converted to dsDNA, end repaired and A tailed. Samples were then ligated to adapters, followed by PCR amplification with indexing primers. Libraries were pooled in equimolar concentrations and sequenced in Illumina NextSeq 500 and 550 sequencers using a high-output cartridge, generating single reads with a length of 75 bp. At least 93% of the reads generated presented a quality score of 30 or above.

The quality of the RNAseq reads was assessed using FastQC (http://www.bioinformatics.babraham.ac.uk/projects/fastqc), and sequence adaptors were removed using TrimGalore (https://www.bioinformatics.babraham.ac.uk/projects/trim_galore). The reference Ovis aries genome (Oar_v3.1) wase downloaded from Ensembl and reads were subsequently aligned using Hisat2[73] and counted using FeatureCount[74], respectively. The EdgeR package was then used to calculate the gene expression levels and to analyse differentially expressed genes[75]. For the *in vivo* experiments, in order to control for background inter-host variation we utilised the dream RNAseq differential expression method[76] implemented in R. This method allows individual-level animal variation to be controlled for using random effects in order to better estimate the impact of treatment (in this case infection) as fixed effects. In order to provide as much data as possible for the model, to estimate the impact of infection we also utilised the uninfected control animals, again each with their own random effects for individual variation. We utilised separate runs to compare each dpi (1,3,7) to dpi 0 using the form 'form <- ~ Disease + (1|Individual)'.

The list of sheep interferon stimulated genes for downstream analysis was taken from Shaw et al. (2017)[51]. The raw FASTQ files associated with this project have been submitted to the European Nucleotide Archive (ENA; project accession number PRJEB72808).

BTV RT-PCR. To determine the amount of viral RNA in the blood of infected and mock-infected animals, RNA samples which were used for sequencing were used for the detection of segment 10 of BTV by RT-qPCR at indicated days post infection. The following probe: 5'-FAM-ARG-CTG-CAT-TCG-CAT-CGT-ACG- C-TAMRA-3', the forward primer: 5'-TGG-AYA-AAG-CRA-TGT-CAA-A-3' and the reverse primer 5'-ACR-TCA-TCA-CGA-AAC-GCT-TC-3' with a thermal profile of: 10 min 50°C, 2 min 95°C, 40x 10 sec 95°C and 30 sec 60°C with the Brilliant III Ultra-Fast qRT-PCR master mix (Agilent, 600884) were used according to manufacturer's protocol.

Histology, immunohistochemistry and image analysis. 2 to 4 um thick sections of formalin fixed and paraffine-embedded (FFPE) tissues from infected and mock-infected animals were cut and mounted on glass slides and stained with haematoxylin and eosin by standard procedures. For the detection of the BTV NS2 protein, a rabbit anti-NS2 antibody was used[77,78] in a dilution of 1:7000. Pre-treatment of tissue sections was carried out by pressure cooking in citrate buffer (pH 6.0) and the EnVision+ Single Reagent (HRP. Mouse, Agilent Technologies, K4001) was used as visualisation system in an autostainer (Autostainer Link 48, Agilent Technologies). As negative control, the primary antibody was replaced by mouse serum. Other antibodies used in the study were the following. Anti-Foxp3 FJK-16s antibody (eBioscience, Thermo Fisher Scientific, 14-5773-82; dilution 1:10); anti-CD3 (Agilent DAKO, A0452; dilution 1:100), anti Ki67 (Agilent DAKO, M724029-2, dilution 1:200), anti-pSTAT-1 (Cell Signalling, 9467S; dilution 1:200), anti-CD163 (Bio-Rad, MCA1853, dilution 1:100), anti-WC-1 (Bio-Rad, MCA838GA, dilution 1:20) and anti-Pax5 (Agilent DAKO, M7307; dilution 1:20). The VECTASTAIN® Elite® ABC HRP Kit (Peroxidase, Rat IgG; Vectorlabs, PK-6104) was used as a secondary system for detecting Foxp3, while for the other antibodies either the EnVision+/HRP, Mouse, HRP kit (Agilent DAKO, K400111-2) or the EnVision+/HRP, Rabbit, HRP kit (Agilent DAKO, K4003) as required. In all experiments, 3,3'-Diaminobenzidine (DAB) was used as a chromogen.

Immunostained slides were scanned with an Aperio VERSA 8 Brightfield, Fluorescence & FISH Digital Pathology Scanner (Leica Biosystems) at 200 x brightfield magnification. To detect the number of immune-positive cells, areas of the following tissues were manually outlined: tongue

(excluding the epithelial mucosa), 3-4 pieces of lung tissue (1-2 pieces frontal lobes, 1-2 pieces distal lobes) per animal, infected skin (left forelimb), non-infected skin (dorsal back), lymph nodes of the infection site (left pre-scapular lymph nodes), liver and spleen. Aperio Software ImageScope (Leica Biosystems) was used to automatically acquire the numbers of positive cells (NS2, CD3, Pax5, CD163, WC-1) or nuclei (Ki67, Foxp3) per total number of cells (NS2, CD3, Pax5, CD163, WC-) or nuclei (Ki67, Foxp3), respectively. In the skin, only the dermis was assessed and data was analysed separately for superficial and deep dermis, while adipose tissue was excluded. For lymph node sections, only the cortex was investigated, while for the spleen, the connective tissue was excluded in the analysis. The whole liver section was instead included. The algorithm and software settings were fine tuned for each organ. Subsequent analyses were carried out using the same setting for each organ. For those organs having more than two tissue sections, the mean value of the two sections was used in subsequent analyses. The mean values obtained from each organ of non-infected animals was used as background value (negative values were transformed to zero), and subtracted to the values obtained from each organ of the infected animals.

Absolute numbers of follicles per lymph node were derived from the right prescapular lymph nodes and were obtained from the average number of follicles obtained from 1 to 3 cross-sections per lymph node stained with HE.

***In situ* hybridization.** FFPE tissue sections were used for the detection of virus-specific RNA by *in situ*-hybridisation. The RNAscope 2.5 HD Reagent Kit-RED (code: 322350, Advanced Cell Diagnostics) and the probes V-BTV-1-ITL-2006KC3-seg4-C1 were designed and purchased (product code: 109711-C11; Advanced Cell Diagnostics). Positive and negative controls included a ubiquitin and a plant gene probe, respectively (codes: 310041 and 310043, Advanced Cell Diagnostics). Assays followed the manufacturer's instructions.

Machine learning. The random forest method for machine learning was used to predict the virus and host parameters correlating with clinical outcome of BTV infection. Random forest was chosen because of the prioritisation metrics built in this method, which allow the most predictive parameters to be discovered and ranked. RandomForest and Caret R packages were used in order to build

583 random forests for prediction (RandomForest function from RandomForest), and the recursive
584 feature elimination algorithm was utilised to find the optimal number of parameters for analysis (rfe
585 function from Caret). In order to find the most consistent predictive parameters, a custom cross-
586 validation approach for predictions was implemented. Firstly, using the whole dataset, parameters
587 were ranked using gini-importance and recursive feature elimination on the top 150 gini parameters
588 were used to see how prediction accuracy varied with the number of parameters available to the
589 random forest model. The value provided by the rfe algorithm was highly variable due to the inherent
590 stochasticity in the algorithm. Hence, the value for parameter number N at the point that the initial
591 slope of accuracy vs parameters began to taper off was chosen; this value was taught to capture the
592 best trade off of accuracy using the fewest parameters. 500 runs of cross-validation were performed
593 using two animals as testing data for each group. Within each of these cross-validation runs, the
594 SMOTE method[79] was used to generate synthetic datapoints to balance predictive groups for the
595 two imbalanced datasets (based on clinical score – "clinical state", or the groupings related to the
596 virus used in the inoculum "four states of infection"). A random forest based on this data was then
597 built, and the N top parameters in each run were recorded. Subsequently, the N parameters which
598 appeared most often in the 500 runs were taken as a final list for that classification model. This list
599 of N parameters was then used as the final set for 500 additional rounds of cross-validation training
600 and testing with 2 holdout testing for each using the previously found N parameters. These runs also
601 utilised SMOTE to balance for the two imbalanced datasets. This gave 1000 testing datapoints
602 (2*500) for each group to show the accuracy of the machine learning predictions. The predictions
603 made during these 500 rounds of cross validation are summarised in the confusion matrices, which
604 show the animal's true state along the columns and predicted values along the rows (see Tables 1-
605 3). To test that our predictions were not the result of over-fitting to the data, we also ran the machine
606 learning modelling script with the rows shuffled, and the individual animals' data randomised across
607 samples and groups. The confusion matrices showing the lack of prediction power of these models
608 can be found in Tables S5-7.

609 **Code availability.** All code used to analyse the data is available at
610 https://github.com/omaclean/sheep_ML (see the readme for specific scripts).

Blood transcriptional modules. In order to combine our 6000 RNA-seq data points with our host and viral-related datapoints without disproportionately weighting the RNA seq results, we compressed the transcriptomics data into 247 blood transcriptional modules. We used the sheep mapped versions from Braun et al.[38] (generously provided by Artur Summerfield in .csv format). For each BTM, we took the geometric mean of each animal's different gene counts' proportion of total transcripts from that sample. These BTM representations of gene expression were further compressed to remove any fully redundant BTMs where one was a fully contained subset of genes of another BTM. We moved BTMs for which we had only one expressed gene in that BTM. We additionally recursively merged any BTMs which were more than 90% Pearson correlated across our dataset (script ~/scripts/R/sheep_mega_data/1.4.21/prep.BTMs.4.8.21.R). This produced a final set of 279* BTMs that we merged with our complete data set, providing a total of 332 parameters for analysis. In order to include postmortem parameters, we were forced to remove BTV-1_{IT2013} animals from the machine learning analysis as they had recovered before these were collected.

Heatmap plotting normalisation. We applied a normalisation per variable, where it's taking the log (x+1) of each value, minus the mean log(x+1) of just the control animals, then divided by the standard deviation of log(x+1) of all the (non-NA) values (in effect a log Z score, but only using the uninfected animals' mean values).

Pathway analysis. Ensembl gene identifiers for each DEG of the blood transcriptome were converted to their respective human orthologue identifier and gene name. Up-regulated high confidence (FDR <0.05) DEGs identified from each pairwise comparison were used for differential pathway analysis in Metascape using *H. sapiens* for species analysis (https://metascape.org/gp/index.html#/main/step1)[80]. Pathway *p*-values <0.05 were considered significant for pathway enrichment. Heat maps were plotted in GraphPad Prism (version 10.2) as log2 mean counts per million (CPM). Missing gene values were plotted as zero.

Statistical analysis. Graphs were created by using R version 4.3.2. or GraphPad Prism version 10.1.2. P-values<0.05 were considered as statistically significant.

Acknowledgements

The authors thank all team members of the Histology Research Service of University of Glasgow: Lynn Stevenson, Frazer Bell, Lynn Oxford, Jan Duncan, and Jessica Lee for the outstanding quality of their work in the histology lab. We also thank Giovanni Antonio Pilo for his invaluable support in the field work. The work would not have been possible without the invaluable help for animal care of Berardo De Dominicis, Doriano Ferrari, Massimiliano Caporale, Giampaolo Foschini in Teramo and the teams in Sassari, Italy. This study was funded by the Wellcome Trust (206369/Z/17/Z) and in part by the EU (H2020 PALE-Blu grant project No: 727393-2), the Italian Ministry of Health (RC IZS SA 02/16 and RC IZS SA 04/18), a Research Fellowship by the Deutsche Forschungsgemeinschaft (DFG; Project number 406109949) and the Medical Research Council (MC_UU_00034/5).

References

1. Cheemarla, N.R., Watkins, T.A., Mihaylova, V.T., Wang, B., Zhao, D., Wang, G., Landry, M.L., and Foxman, E.F. (2021). Dynamic innate immune response determines susceptibility to SARS-CoV-2 infection and early replication kinetics. J Exp Med *218*. 10.1084/jem.20210583.
2. Fried, J.R., Gibbons, R.V., Kalayanarooj, S., Thomas, S.J., Srikiatkhachorn, A., Yoon, I.K., Jarman, R.G., Green, S., Rothman, A.L., and Cummings, D.A. (2010). Serotype-specific differences in the risk of dengue hemorrhagic fever: an analysis of data collected in Bangkok, Thailand from 1994 to 2006. PLoS Negl Trop Dis *4*, e617. 10.1371/journal.pntd.0000617.
3. Karim, S.S.A., and Karim, Q.A. (2021). Omicron SARS-CoV-2 variant: a new chapter in the COVID-19 pandemic. Lancet *398*, 2126-2128. 10.1016/S0140-6736(21)02758-6.
4. Quan, C., Shi, W., Yang, Y., Yang, Y., Liu, X., Xu, W., Li, H., Li, J., Wang, Q., Tong, Z., et al. (2018). New Threats from H7N9 Influenza Virus: Spread and Evolution of High- and Low-Pathogenicity Variants with High Genomic Diversity in Wave Five. J Virol *92*. 10.1128/JVI.00301-18.
5. Schultze, J.L., and Aschenbrenner, A.C. (2021). COVID-19 and the human innate immune system. Cell *184*, 1671-1692. 10.1016/j.cell.2021.02.029.
6. Clohisey, S., and Baillie, J.K. (2019). Host susceptibility to severe influenza A virus infection. Crit Care *23*, 303. 10.1186/s13054-019-2566-7.
7. Hua, C., and Combe, B. (2017). Chikungunya Virus-Associated Disease. Curr Rheumatol Rep *19*, 69. 10.1007/s11926-017-0694-0.
8. Zhang, H., Zhou, P., Wei, Y., Yue, H., Wang, Y., Hu, M., Zhang, S., Cao, T., Yang, C., Li, M., et al. (2020). Histopathologic Changes and SARS-CoV-2 Immunostaining in the Lung of a Patient With COVID-19. Ann Intern Med. 10.7326/M20-0533.
9. Lopez, L., Sang, P.C., Tian, Y., and Sang, Y. (2020). Dysregulated Interferon Response Underlying Severe COVID-19. Viruses *12*. 10.3390/v12121433.
10. Chen, G., Wu, D., Guo, W., Cao, Y., Huang, D., Wang, H., Wang, T., Zhang, X., Chen, H., Yu, H., et al. (2020). Clinical and immunological features of severe and moderate coronavirus disease 2019. J Clin Invest *130*, 2620-2629. 10.1172/jci137244.
11. Wickenhagen, A., Sugrue, E., Lytras, S., Kuchi, S., Noerenberg, M., Turnbull, M.L., Loney, C., Herder, V., Allan, J., Jarmson, I., et al. (2021). A prenylated dsRNA sensor protects against severe COVID-19. Science *374*, eabj3624. 10.1126/science.abj3624.
12. Zhang, H., Zhou, P., Wei, Y., Yue, H., Wang, Y., Hu, M., Zhang, S., Cao, T., Yang, C., Li, M., et al. (2020). Histopathologic Changes and SARS-CoV-2 Immunostaining in the Lung of a Patient With COVID-19. Ann Intern Med *172*, 629-632. 10.7326/m20-0533.

13. Carrington, M., Dean, M., Martin, M.P., and O'Brien, S.J. (1999). Genetics of HIV-1 infection: chemokine receptor CCR5 polymorphism and its consequences. Hum Mol Genet *8*, 1939-1945. 10.1093/hmg/8.10.1939.

14. Mehlotra, R.K. (2020). Chemokine receptor gene polymorphisms and COVID-19: Could knowledge gained from HIV/AIDS be important? Infect Genet Evol *85*, 104512. 10.1016/j.meegid.2020.104512.

15. Pairo-Castineira, E., Clohisey, S., Klaric, L., Bretherick, A.D., Rawlik, K., Pasko, D., Walker, S., Parkinson, N., Fourman, M.H., Russell, C.D., et al. (2021). Genetic mechanisms of critical illness in COVID-19. Nature *591*, 92-98. 10.1038/s41586-020-03065-y.

16. Guzman, M.G., and Harris, E. (2015). Dengue. Lancet *385*, 453-465. 10.1016/S0140-6736(14)60572-9.

17. Ortego, J., de la Poza, F., and Marin-Lopez, A. (2014). Interferon alpha/beta receptor knockout mice as a model to study bluetongue virus infection. Virus Res *182*, 35-42. 10.1016/j.virusres.2013.09.038.

18. Kenney, A.D., McMichael, T.M., Imas, A., Chesarino, N.M., Zhang, L., Dorn, L.E., Wu, Q., Alfaour, O., Amari, F., Chen, M., et al. (2019). IFITM3 protects the heart during influenza virus infection. Proc Natl Acad Sci U S A *116*, 18607-18612. 10.1073/pnas.1900784116.

19. Maclachlan, N.J. (2011). Bluetongue: history, global epidemiology, and pathogenesis. Prev Vet Med *102*, 107-111. 10.1016/j.prevetmed.2011.04.005.

20. Schulz, C., Breard, E., Sailleau, C., Jenckel, M., Viarouge, C., Vitour, D., Palmarini, M., Gallois, M., Hoper, D., Hoffmann, B., et al. (2016). Bluetongue virus serotype 27: detection and characterization of two novel variants in Corsica, France. J Gen Virol *97*, 2073-2083. 10.1099/jgv.0.000557.

21. Schulz, C., Eschbaumer, M., Rudolf, M., Konig, P., Keller, M., Bauer, C., Gauly, M., Grevelding, C.G., Beer, M., and Hoffmann, B. (2012). Experimental infection of South American camelids with bluetongue virus serotype 8. Vet Microbiol *154*, 257-265. 10.1016/j.vetmic.2011.07.025.

22. Schulz, C., Sailleau, C., Breard, E., Flannery, J., Viarouge, C., Zientara, S., Beer, M., Batten, C., and Hoffmann, B. (2018). Experimental infection of sheep, goats and cattle with a bluetongue virus serotype 4 field strain from Bulgaria, 2014. Transbound Emerg Dis *65*, e243-e250. 10.1111/tbed.12746.

23. Ries, C., Sharav, T., Tseren-Ochir, E.O., Beer, M., and Hoffmann, B. (2020). Putative Novel Serotypes '33' and '35' in Clinically Healthy Small Ruminants in Mongolia Expand the Group of Atypical BTV. Viruses *13*. 10.3390/v13010042.

24. Ries, C., Vogtlin, A., Hussy, D., Jandt, T., Gobet, H., Hilbe, M., Burgener, C., Schweizer, L., Hafliger-Speiser, S., Beer, M., and Hoffmann, B. (2021). Putative Novel Atypical BTV Serotype '36' Identified in Small Ruminants in Switzerland. Viruses *13*. 10.3390/v13050721.

25. Melle Holwerda, I.M.G.A.S.-B., Frank Harders, Marc Engelsma, Rianka P.M. Vloet, Eveline Dijkstra, Rene G.P. van Gennip, Maria H. Mars, Marcel Spierenburg, Lotte Roos, René van den Brom, Piet A. van Rijn (2023). Emergence of bluetongue virus serotype 3 in the Netherlands in September 2023. bioRxiv preprint. doi: https://doi.org/10.1101/2023.09.29.560138

26. Alkhamis, M.A., Aguilar-Vega, C., Fountain-Jones, N.M., Lin, K., Perez, A.M., and Sanchez-Vizcaino, J.M. (2020). Global emergence and evolutionary dynamics of bluetongue virus. Sci Rep *10*, 21677. 10.1038/s41598-020-78673-9.

27. Barry, G., Varela, M., Ratinier, M., Blomstrom, A.L., Caporale, M., Seehusen, F., Hahn, K., Schnettler, E., Baumgartner, W., Kohl, A., and Palmarini, M. (2014). The NSs protein of Schmallenberg virus counteracts the antiviral response of the cell by inhibiting its transcriptional machinery. J Gen Virol. 10.1099/vir.0.065425-0.

28. Darpel, K.E., Batten, C.A., Veronesi, E., Shaw, A.E., Anthony, S., Bachanek-Bankowska, K., Kgosana, L., bin-Tarif, A., Carpenter, S., Muller-Doblies, U.U., et al. (2007). Clinical signs and pathology shown by British sheep and cattle infected with bluetongue virus serotype 8 derived from the 2006 outbreak in northern Europe. Vet Rec *161*, 253-261.

29. Erasmus, B.J. (1975). Bluetongue in sheep and goats. Aust Vet J *51*, 165-170.

30. Howell, P.G., and Verwoerd, D.W. (1971). Bluetongue virus. Virol Monogr *9*, 35-74.

31. Maclachlan, N.J., Drew, C.P., Darpel, K.E., and Worwa, G. (2009). The pathology and pathogenesis of bluetongue. J Comp Pathol *141*, 1-16. 10.1016/j.jcpa.2009.04.003.

32. Melzi, E., Caporale, M., Rocchi, M., Martin, V., Gamino, V., di Provvido, A., Marruchella, G., Entrican, G., Sevilla, N., and Palmarini, M. (2016). Follicular dendritic cell disruption as a novel mechanism of virus-induced immunosuppression. Proceedings of the National Academy of Sciences of the United States of America *113*, E6238-E6247. 10.1073/pnas.1610012113.

33. Bean, A.G., Baker, M.L., Stewart, C.R., Cowled, C., Deffrasnes, C., Wang, L.F., and Lowenthal, J.W. (2013). Studying immunity to zoonotic diseases in the natural host - keeping it real. Nat Rev Immunol *13*, 851-861. 10.1038/nri3551.

34. Rajkomar, A., Dean, J., and Kohane, I. (2019). Machine Learning in Medicine. N Engl J Med *380*, 1347-1358. 10.1056/NEJMra1814259.

35. Puggioni, G., Pintus, D., Meloni, G., Scivoli, R., Rocchigiani, A.M., Manunta, D., Savini, G., Oggiano, A., and Ligios, C. (2018). Persistence of Bluetongue virus serotype 1 virulence in sheep blood refrigerated for 10 years. Vet Ital *54*, 349-353. 10.12834/VetIt.1344.7401.3.

36. Puggioni, G., Pintus, D., Melzi, E., Meloni, G., Rocchigiani, A.M., Maestrale, C., Manunta, D., Savini, G., Dattena, M., Oggiano, A., et al. (2018). Testicular Degeneration and Infertility following Arbovirus Infection. J Virol *92*. 10.1128/JVI.01131-18.

37. Caporale, M., Di Gialleonorado, L., Janowicz, A., Wilkie, G., Shaw, A., Savini, G., Van Rijn, P.A., Mertens, P., Di Ventura, M., and Palmarini, M. (2014). Virus and host factors affecting the clinical outcome of bluetongue virus infection. J Virol *88*, 10399-10411. 10.1128/JVI.01641-14.

38. Braun, R.O., Brunner, L., Wyler, K., Auray, G., Garcia-Nicolas, O., Python, S., Zumkehr, B., Gaschen, V., Stoffel, M.H., Collin, N., et al. (2018). System immunology-based identification of blood transcriptional modules correlating to antibody responses in sheep. NPJ Vaccines *3*, 41. 10.1038/s41541-018-0078-0.

39. Li, S., Rouphael, N., Duraisingham, S., Romero-Steiner, S., Presnell, S., Davis, C., Schmidt, D.S., Johnson, S.E., Milton, A., Rajam, G., et al. (2014). Molecular signatures of antibody responses derived from a systems biology study of five human vaccines. Nat Immunol *15*, 195-204. 10.1038/ni.2789.

40. Nembrini, S., Konig, I.R., and Wright, M.N. (2018). The revival of the Gini importance? Bioinformatics *34*, 3711-3718. 10.1093/bioinformatics/bty373.

41. Chatzinasiou, E., Chaintoutis, S.C., Dovas, C.I., Papanastassopoulou, M., and Papadopoulos, O. (2017). Immunosuppression in sheep induced by cyclophosphamide, bluetongue virus and their combination: Effect on clinical reaction and viremia. Microb Pathog *104*, 318-327. 10.1016/j.micpath.2017.01.048.

42. Rodriguez-Martin, D., Louloudes-Lazaro, A., Avia, M., Martin, V., Rojas, J.M., and Sevilla, N. (2021). The Interplay between Bluetongue Virus Infections and Adaptive Immunity. Viruses *13*. 10.3390/v13081511.

43. Rouse, B.T., Sarangi, P.P., and Suvas, S. (2006). Regulatory T cells in virus infections. Immunol Rev *212*, 272-286. 10.1111/j.0105-2896.2006.00412.x.

44. Veiga-Parga, T., Sehrawat, S., and Rouse, B.T. (2013). Role of regulatory T cells during virus infection. Immunol Rev *255*, 182-196. 10.1111/imr.12085.

45. Shepard, D.S., Undurraga, E.A., Halasa, Y.A., and Stanaway, J.D. (2016). The global economic burden of dengue: a systematic analysis. Lancet Infect Dis *16*, 935-941. 10.1016/s1473-3099(16)00146-8.

46. Bente, D.A., Forrester, N.L., Watts, D.M., McAuley, A.J., Whitehouse, C.A., and Bray, M. (2013). Crimean-Congo hemorrhagic fever: history, epidemiology, pathogenesis, clinical syndrome and genetic diversity. Antiviral Res *100*, 159-189. 10.1016/j.antiviral.2013.07.006.

47. Musso, D., and Gubler, D.J. (2016). Zika Virus. Clin Microbiol Rev *29*, 487-524. 10.1128/CMR.00072-15.

48. Sippy, R., Farrell, D.F., Lichtenstein, D.A., Nightingale, R., Harris, M.A., Toth, J., Hantztidiamantis, P., Usher, N., Cueva Aponte, C., Barzallo Aguilar, J., et al. (2020). Severity Index for Suspected Arbovirus (SISA): Machine learning for accurate prediction of

hospitalization in subjects suspected of arboviral infection. PLoS Negl Trop Dis *14*, e0007969. 10.1371/journal.pntd.0007969.

49. Shu, T., Ning, W., Wu, D., Xu, J., Han, Q., Huang, M., Zou, X., Yang, Q., Yuan, Y., Bie, Y., et al. (2020). Plasma Proteomics Identify Biomarkers and Pathogenesis of COVID-19. Immunity *53*, 1108-1122.e1105. 10.1016/j.immuni.2020.10.008.

50. Filho, J.D.S., Herder, V., Gibbins, M.P., Reis, M.F.d., Melo, G.C., Haley, M.J., Judice, C.C., Val, F.F.A., Borba, M., Tavella, T.A., et al. (2023). Disease trajectories in hospitalized COVID-19 patients are predicted by clinical and peripheral blood signatures representing distinct lung pathologies. medRxiv, 2023.2009.2008.23295024. 10.1101/2023.09.08.23295024.

51. Shaw, A.E., Hughes, J., Gu, Q., Behdenna, A., Singer, J.B., Dennis, T., Orton, R.J., Varela, M., Gifford, R.J., Wilson, S.J., and Palmarini, M. (2017). Fundamental properties of the mammalian innate immune system revealed by multispecies comparison of type I interferon responses. PLoS biology *15*, e2004086. 10.1371/journal.pbio.2004086.

52. Hardy, A., Bakshi, S., Furnon, W., MacLean, O., Gu, Q., Varjak, M., Varela, M., Aziz, M.A., Shaw, A.E., Pinto, R.M., et al. (2023). The Timing and Magnitude of the Type I Interferon Response Are Correlated with Disease Tolerance in Arbovirus Infection. mBio *14*, e0010123. 10.1128/mbio.00101-23.

53. Li, Z., Lu, D., Yang, H., Li, Z., Zhu, P., Xie, J., Liao, D., Zheng, Y., and Li, H. (2021). Bluetongue virus non-structural protein 3 (NS3) and NS4 coordinatively antagonize type Ⅰ interferon signaling by targeting STAT1. Vet Microbiol *254*, 108986. 10.1016/j.vetmic.2021.108986.

54. Ratinier, M., Caporale, M., Golder, M., Franzoni, G., Allan, K., Nunes, S.F., Armezzani, A., Bayoumy, A., Rixon, F., Shaw, A., and Palmarini, M. (2011). Identification and characterization of a novel non-structural protein of bluetongue virus. PLoS Pathog *7*, e1002477. 10.1371/journal.ppat.1002477.

55. Ratinier, M., Shaw, A.E., Barry, G., Gu, Q., Di Gialleonardo, L., Janowicz, A., Varela, M., Randall, R.E., Caporale, M., and Palmarini, M. (2016). Bluetongue Virus NS4 Protein Is an Interferon Antagonist and a Determinant of Virus Virulence. J Virol *90*, 5427-5439. 10.1128/JVI.00422-16.

56. Chauveau, E., Doceul, V., Lara, E., Breard, E., Sailleau, C., Vidalain, P.O., Meurs, E.F., Dabo, S., Schwartz-Cornil, I., Zientara, S., and Vitour, D. (2013). NS3 of bluetongue virus interferes with the induction of type I interferon. J Virol *87*, 8241-8246. 10.1128/JVI.00678-13.

57. Vitour, D., Doceul, V., Ruscanu, S., Chauveau, E., Schwartz-Cornil, I., and Zientara, S. (2014). Induction and control of the type I interferon pathway by Bluetongue virus. Virus Res *182*, 59-70. 10.1016/j.virusres.2013.10.027.

58. Liu, M., Guo, S., Hibbert, J.M., Jain, V., Singh, N., Wilson, N.O., and Stiles, J.K. (2011). CXCL10/IP-10 in infectious diseases pathogenesis and potential therapeutic implications. Cytokine Growth Factor Rev *22*, 121-130. 10.1016/j.cytogfr.2011.06.001.

59. Malavige, G.N., and Ogg, G.S. (2017). Pathogenesis of vascular leak in dengue virus infection. Immunology *151*, 261-269. 10.1111/imm.12748.

60. Louloudes-Lazaro, A., Rojas, J.M., Garcia-Garcia, I., Rodriguez-Martin, D., Morel, E., Martin, V., and Sevilla, N. (2023). Comprehensive immune profiling reveals that Orbivirus infection activates immune checkpoints during acute T cell immunosuppression. Front Immunol *14*, 1255803. 10.3389/fimmu.2023.1255803.

61. Melzi, E., Caporale, M., Rocchi, M., Martin, V., Gamino, V., di Provvido, A., Marruchella, G., Entrican, G., Sevilla, N., and Palmarini, M. (2016). Follicular dendritic cell disruption as a novel mechanism of virus-induced immunosuppression. Proc Natl Acad Sci U S A *113*, E6238-E6247. 10.1073/pnas.1610012113.

62. McColl, K.A., and Gould, A.R. (1994). Bluetongue virus infection in sheep: haematological changes and detection by polymerase chain reaction. Aust Vet J *71*, 97-101. 10.1111/j.1751-0813.1994.tb03346.x.

63. Ciurkiewicz, M., Herder, V., and Beineke, A. (2020). Beneficial and Detrimental Effects of Regulatory T Cells in Neurotropic Virus Infections. Int J Mol Sci *21*. 10.3390/ijms21051705.

64. Procaccini, C., Garavelli, S., Carbone, F., Di Silvestre, D., La Rocca, C., Greco, D., Colamatteo, A., Lepore, M.T., Russo, C., De Rosa, G., et al. (2021). Signals of pseudo-starvation unveil the amino acid transporter SLC7A11 as key determinant in the control of Treg cell proliferative potential. Immunity *54*, 1543-1560 e1546. 10.1016/j.immuni.2021.04.014.

65. Veiga-Parga, T., Suryawanshi, A., Mulik, S., Gimenez, F., Sharma, S., Sparwasser, T., and Rouse, B.T. (2012). On the role of regulatory T cells during viral-induced inflammatory lesions. J Immunol *189*, 5924-5933. 10.4049/jimmunol.1202322.

66. Zhao, J., Zhao, J., and Perlman, S. (2014). Virus-specific regulatory T cells ameliorate encephalitis by repressing effector T cell functions from priming to effector stages. PLoS Pathog *10*, e1004279. 10.1371/journal.ppat.1004279.

67. Anghelina, D., Zhao, J., Trandem, K., and Perlman, S. (2009). Role of regulatory T cells in coronavirus-induced acute encephalitis. Virology *385*, 358-367. 10.1016/j.virol.2008.12.014.

68. Wechsler, S.J., McHolland, L.E., and Tabachnick, W.J. (1989). Cell lines from Culicoides variipennis (Diptera: Ceratopogonidae) support replication of bluetongue virus. J Invertebr Pathol *54*, 385-393. 10.1016/0022-2011(89)90123-7.

69. Shaw, A.E., Ratinier, M., Nunes, S.F., Nomikou, K., Caporale, M., Golder, M., Allan, K., Hamers, C., Hudelet, P., Zientara, S., et al. (2013). Reassortment between two serologically

unrelated bluetongue virus strains is flexible and can involve any genome segment. J Virol *87*, 543-557. 10.1128/JVI.02266-12.

70. Nunes, S.F., Hamers, C., Ratinier, M., Shaw, A., Brunet, S., Hudelet, P., and Palmarini, M. (2014). A synthetic biology approach for a vaccine platform against known and newly emerging serotypes of bluetongue virus. J Virol *88*, 12222-12232. 10.1128/JVI.02183-14.
71. Arnaud, F., Black, S.G., Murphy, L., Griffiths, D.J., Neil, S.J., Spencer, T.E., and Palmarini, M. (2010). Interplay between ovine bone marrow stromal cell antigen 2/tetherin and endogenous retroviruses. J Virol *84*, 4415-4425. 10.1128/JVI.00029-10.
72. Lelli, R., Di Ventura, M., Mercante, M.T., Tittarelli, M., Mangana-Vougiouka, O., Nomikou, K., Conte, A., Di Emidio, B., Portanti, O., Giovannucci, G., et al. (2004). Bluetongue laboratory diagnosis: a ring test to evaluate serological results using a competitive ELISA kit. Vet Ital *40*, 577-580.
73. Kim, D., Langmead, B., and Salzberg, S.L. (2015). HISAT: a fast spliced aligner with low memory requirements. Nature methods *12*, 357-360. 10.1038/nmeth.3317.
74. Liao, Y., Smyth, G.K., and Shi, W. (2014). featureCounts: an efficient general purpose program for assigning sequence reads to genomic features. Bioinformatics *30*, 923-930. 10.1093/bioinformatics/btt656.
75. Robinson, M.D., McCarthy, D.J., and Smyth, G.K. (2010). edgeR: a Bioconductor package for differential expression analysis of digital gene expression data. Bioinformatics *26*, 139-140. 10.1093/bioinformatics/btp616.
76. Hoffman, G.E., and Roussos, P. (2021). Dream: powerful differential expression analysis for repeated measures designs. Bioinformatics *37*, 192-201. 10.1093/bioinformatics/btaa687.
77. Caporale, M., Wash, R., Pini, A., Savini, G., Franchi, P., Golder, M., Patterson-Kane, J., Mertens, P., Di Gialleonardo, L., Armillotta, G., et al. (2011). Determinants of bluetongue virus virulence in murine models of disease. J Virol *85*, 11479-11489. 10.1128/JVI.05226-11JVI.05226-11 [pii].
78. Gold, S., Monaghan, P., Mertens, P., and Jackson, T. (2010). A clathrin independent macropinocytosis-like entry mechanism used by bluetongue virus-1 during infection of BHK cells. PLoS One *5*, e11360. 10.1371/journal.pone.0011360.
79. Chawla, N.V., Bowyer, K.W., Hall, L.O., Kegelmeyer, W.P. (2002). SMOTE: Synthetic Minority Over-sampling Technique. Journal Of Artificial Intelligence Research *16*, 321-357. https://doi.org/10.1613/jair.953.
80. Zhou, Y., Zhou, B., Pache, L., Chang, M., Khodabakhshi, A.H., Tanaseichuk, O., Benner, C., and Chanda, S.K. (2019). Metascape provides a biologist-oriented resource for the analysis of systems-level datasets. Nat Commun *10*, 1523. 10.1038/s41467-019-09234-6.

Figure legends

Figure 1. Distinct clinical phenotypes in experimentally induced bluetongue. (a-c) Images of sheep experimentally infected with different strains of BTV in location G1. (a-b) Rams within the G1-BTV-1-2006 group displaying severe subcutaneous oedema in the neck (a), or ulcerations and crusts of the nostrils and surrounding skin (b). (c) Healthy mock-infected G1-control ram. (d-f) Images of sheep experimentally infected with different strains of BTV in location G2. (d) Mock-infected female G2-control sheep. (e) Female sheep (G2-BTV-1-2006) with a moderate subcutaneous oedema of the head and nose bridge. (f) Mild, focal ulceration on the nostril of a female sheep (G2-BTV-1-2013. (g-h) Clinical score and rectal temperature of all experimentally infected sheep and control used in this study. 2-way ANOVA, **=p<0.01. Data are shown as the median, with minimum and maximum observed values. Grey lines indicate the upper and lower reference value for the physiological rectal temperature in sheep.

Figure 2. Selection of core subsets of predictive correlates of disease severity. Using 332 parameters obtained from each animal in this study, we used a supervised machine learning approach to identify the most predictive core subset of parameters distinguishing each group. The datasets were grouped in three distinct ways: (a) 6 states of infection (groups distinguished on the bases of virus and location used in this study), (b) 4 states of infection (groups distinguished on the bases of the virus used only), and (c) clinical states (groups distinguished on the bases of their clinical scores only). 50 parameters show a prediction accuracy of more than 90 % for the 6 states of infection. 17 parameters show a prediction accuracy of more than 90 % for the 4 states of infection, while 100 parameters show a prediction accuracy of more than 65 % for the clinical states of infection. Note full y-axis on the left side, while the right side is zoomed in for clarity. The accuracy for the clinical scores is likely inflated by the imbalanced group sizes, thus the greater discrepancy between accuracy and kappa. Accuracy = proportion of samples correctly assigned; kappa= Cohen's Kappa: adjusted prediction accuracy to reflect the expected performance of random guesses & account for imbalanced classes; best subset= highest accuracy of any individual run; used subset= selected number of parameters for further analyses.

Figure 3. Key parameters defining the clinical outcome of bluetongue. (a) Core parameters defined as those with the highest gini-importance number that are common to at least two of the three groupings analysed in Fig. 2. Arrows indicate the 8 parameters identified in all three groupings. (b) Brief description of the core parameters shown in a. Note that M68 (identified by an asterisk) is merged with similar BTMs containing overlapping sets of genes. (c) Heatmap showing the relative quantification of the 35 parameters divided by group and individual animals used in this study. Black boxes indicate when the values were not available. Top numerical row indicates the clinical scores of individual animals.

Figure 4. Viral replication in blood and tissues of infected animals. (a) Scatter dot plot showing levels of BTV RNA obtained by qRT-PCR in blood samples. Data indicate medians with minimum and maximum values. Statistical significance between groups was measured by unpaired t-test (* is p=<0.05, ** is p=<0.01). (b) Heatmap displaying the relative amount of BTV NS2 protein in tissues collected from infected animals at 7 days post-infection. Values were obtained by relative quantification of positive signal from immunohistochemistry of whole tissue section slides and downstream software-assisted image analysis as described in Methods. Data are normalised to average obtained in control animals. (c) Immunohistochemistry of tissue section from the tongue of a sheep within the G1-BTV-1-2006 group showing viral NS2 (brown signal, arrows) in endothelial cells of arteries and veins (bar = 100 µm). (d) *In situ* hybridisation of tissue section from the tongue of a sheep within the G1-BTV-1-2006 group revealing the presence of viral RNA in endothelial cells of an artery (red signal, arrow); Asterisk in the insert highlights more endothelial cells with a positive signal for viral RNA. Bar insert = 50 µm; bar main panel = 100 µm. (e-h) Immunohistochemistry in tissue sections derived from skin of infected animals at the inoculation sites showing viral NS2 (brown signal, arrow) in endothelial cells. Images representative of skin samples from animals in group G1-BTV-1-2006 (e), G2-BTV-1-2006 (f), G2-BTV-1-2013 (g); G2-BTV-8 (h); Bars = 60 µm. (i) Confocal microscope images from skin (inoculation site) tissue sections of a sheep infected with BTV-1_{IT2006} collected at 2 dpi. Virus NS2 (green) is detected in lymphatic endothelial cells infected cells as highlighted with antibody towards Lyve-1 (red). Cell nuclei are shown in blue (bars = 10 µm).

Figure 5. Early modulation of ISGs upregulation correlates with disease severity. (a) Scatter dot plots illustrating systemic ISGs upregulation in infected animals (normalised to mock-infected controls). Data were obtained by RNAseq from the blood at 1, 3 and 7 days post infection (dpi). Numbers on top of each graph illustrate the number of significantly upregulated ISGs (FDR < 0.05), showed as bright coloured dots compared to grey background). Note that animals in location G1 infected with BTV-1_{IT2006} show no ISG upregulation at early timepoints (1 dpi), while show the largest number of differentially regulated ISGs at later time points. (b) Scatter plots showing upregulation of ISGs in endothelial cells infected *in vitro* with either BTV-8_{FR2017}, BTV-1_{IT2013}, or BTV-1_{IT2006} compared to uninfected mock controls. Numbers on top of each graph illustrate the number of significantly upregulated ISGs (FDR < 0.05), showed as bright coloured dots compared to grey background).

Figure 6. Extent of pro-inflammatory response, protein loss and lymphopenia correlate with disease severity. (a) Levels of pro-inflammatory markers (MCP-1, CXCL-10/IP-10, IFN-ɣ) in the serum of infected and mock-infected animals at 7 days post-infection (dpi). Data for each animals are normalised to levels at day 0. (b) Level of total proteins in the sera of infected and mock-infected controls during the course of the experiment. Red and blue asterisks indicate statistical differences compared to mock. For the statistical differences in location G2 the asterisks indicates multiple comparisons: 4 dpi=G2-BTV-1-2013 vs. G2-BTV-1-2006 p=0.0024, G2-BTV-1-2013 vs. G2-BTV-8 p=0.0158, G2-BTV-1-2006 vs. G2-BTV-8 p=0.0143; 5 dpi= G2-BTV-1-2013 vs. G2-BTV-1-2006 p=0.0286, G2-BTV-1-2013 vs. G2-BTV-8 p=0.0233; 6 dpi= G2-BTV-1-2013 vs. G2-BTV-1-2006 p=0.0298; 7 dpi= G2-control v. G2-BTV-1-2006 p=0.0234; G2-BTV-1-2013 vs. G2-BTV-1-2006 p=0.0019, G2-BTV-1-2006 vs. G2-BTV-8 p=0.0205. (c) Lymphopenia shown as reduced lymphocyte counts in the blood of sheep with severe disease (G1-BTV-1-2006) compared to mock-infected controls. Black asterisks indicate differences between G1-BTV-1-2006 and mock. (d) Top panels, photomicrographs of lymph node sections stained with haematoxylin and eosin and quantification. Some follicles are highlighted with asterisks. Black line indicates the border between the lymph node cortex and medulla. Bars = 1 mm. Bottom panel, number of follicles in the cross-section of a lymph node draining the site of virus inoculation . Significant difference is shown between G1-BTV-1-2006 and G1-BTV-1-2013. (e) Top panels, immunohistochemistry of lymph node sections stained with an

antibody for the nuclear marker Foxp3. Bars= 200µm. Bottom panel, measurement of Foxp3-positive cells by software-assisted image analysis in lymph node sections. All graphs: Data are shown as the median, with minimum and maximum observed values. 2-way ANOVA, *=p<0.05; **=p<0.01; ***=p<0.001; ****=p<0.0001.

Figure 7. Schematic representation of the key pathogenetic mechanisms of bluetongue pathogenesis. The virus replicates in the sites of virus inoculation and then in the regional lymph nodes, before entering the blood compartment and reaching the peripheral organs. Animals with severe disease are characterised by a late IFN response, high proinflammatory mediators, reduced blood proteins, high viraemia and viral replication in peripheral organs.

Figure S1. Clinical outcome of BTV-1$_{IT2006}$ infection in male and female sheep. Three additional rams were experimentally infected in location G2 and compared to female sheep. (a) Clinical signs. Note significant difference in the severity of clinical signs in infected rams compared to ewes at 6 dpi (p=0.0344; 2-way-ANOVA). (b) Body temperature. Only male animals infected with BTV-1 2006 have a fever peak at 3 dpi compared to all other groups; no significant differences between male and female animals infected with BTV-1 2006 have been detected at any time point. Data are shown as median, minimum and maximum values.

Figure S2: BTV infection induces the differential regulation of host pro-inflammatory immune defences in a strain specific manner. RNA was extracted from BTV infected sheep at 7 days post infection (dpi) and used for RNA-Seq. Host reads were aligned to the sheep genome and normalised to their corresponding negative control group (counts per million; CPM). Differentially expressed genes (adjusted *p*-value < 0.05; FDR) were identified for each pairwise comparison (as indicated). (a) Metascape pathway analysis of up-regulated DEGs showing relative pathway enrichment for each pairwise comparison (*p*-value < 0.05; log10 *p*-values shown). Top 25 pathways shown (ranked on G1-BTV-1-2006). (b-d) Expression profile (mean log2 CPM) of host DEGs identified during BTV infection associated with DisGeNET inflammation (C0021368), vascular disease (C0042373), and immune suppression (C4048329) pathways. Missing values are plotted as zero. *P*-values and test shown.

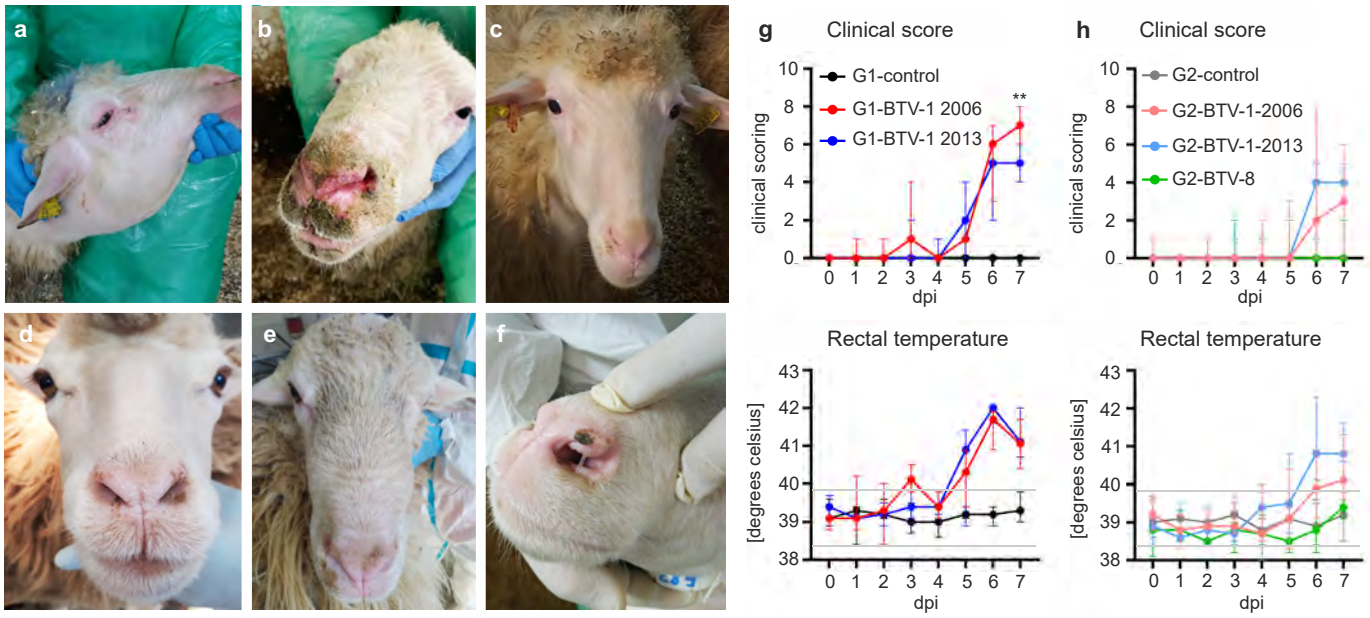

Fig. 1

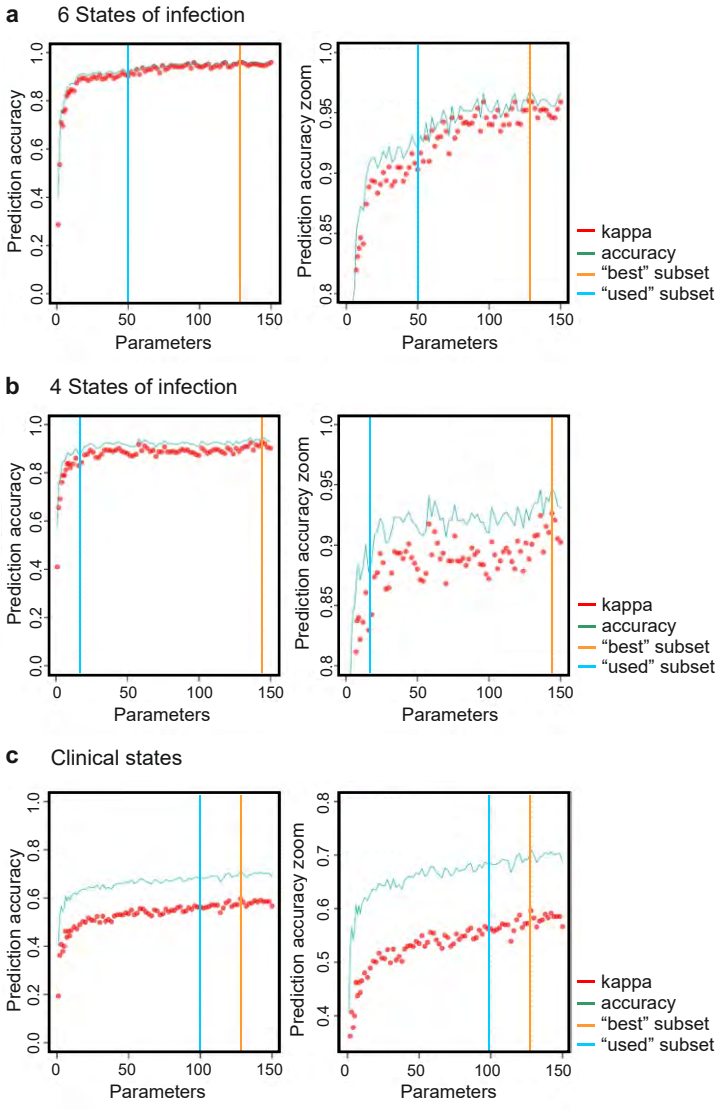

Fig. 2

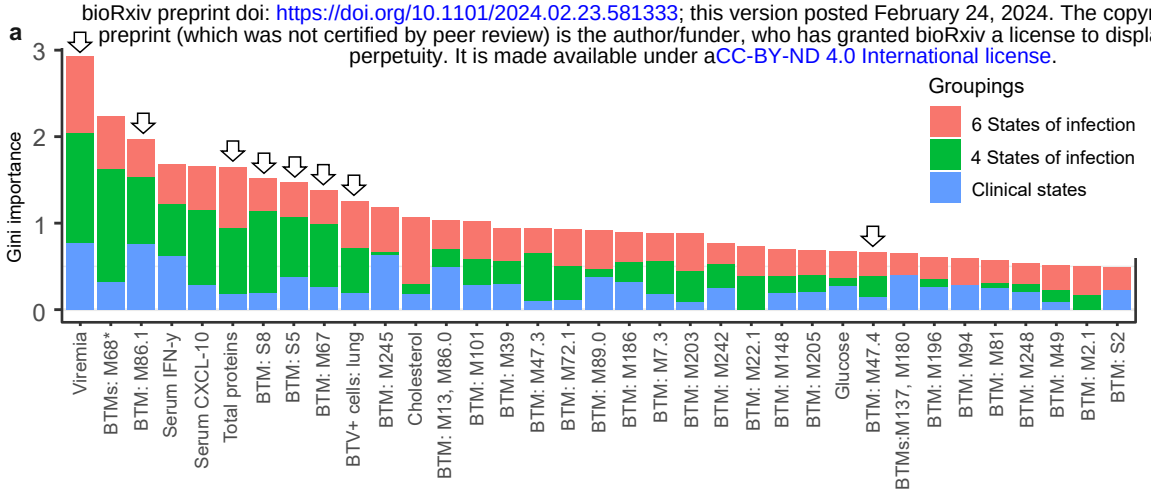

Fig. 3

b

Parameter	Description	Parameter	Description
Viremia	Viral RNA in the blood (RTq-PCR)	**BTM: M186**	Not defined
BTM: M68*	Antiviral and interferon genes	**BTM: M7.3**	T cell activation
BTM: M86.1	Proinflammatory genes	**BTM: M203**	Not defined
Serum IFN-y	IFN-y in the blood	**BTM: M242**	Not defined
Serum CXCL-10	IP-10 in the blood	**BTM: M22.1**	Mismatch repair
Total proteins	Total protein in the blood	**BTM: M148**	Not defined
BTM: S8	Naïve B cell surface signature	**BTM: M205**	Not defined
BTM: S5	Dendritic cell surface signature	**Glucose**	Glucose in the blood
BTM: M67	Activated dendritic cells	**BTM: M47.4**	Enriched in B cells
BTV⁺ cells: lung	NS2⁺ cells IHC	**BTMs: M137, M180**	Not defined
BTM: M245	Translation initiation	**BTM: M196**	Platelet activation
Cholesterol	Cholesterol in the blood	**BTM: M94**	Growth factor induced
BTM: M13, M86.0	Chemokines, inflammatory, innate activation	**BTM: M81**	Enriched in myeloid cells and monocytes
BTM: M101	Phosphatidylinositol signalling system	**BTM: M248**	Not definded
BTM: M39	Integrin mediated leukocyte migration	**BTM: M49**	Transcription regulation in cell development
BTM: M47.3	Enriched in B cells	**BTM: M2.1**	Extracellular matrix
BTM: M72.1	Not defined	**BTM: S2**	B cell surface signature
BTM: M89.0	Putative targets of PAX3		

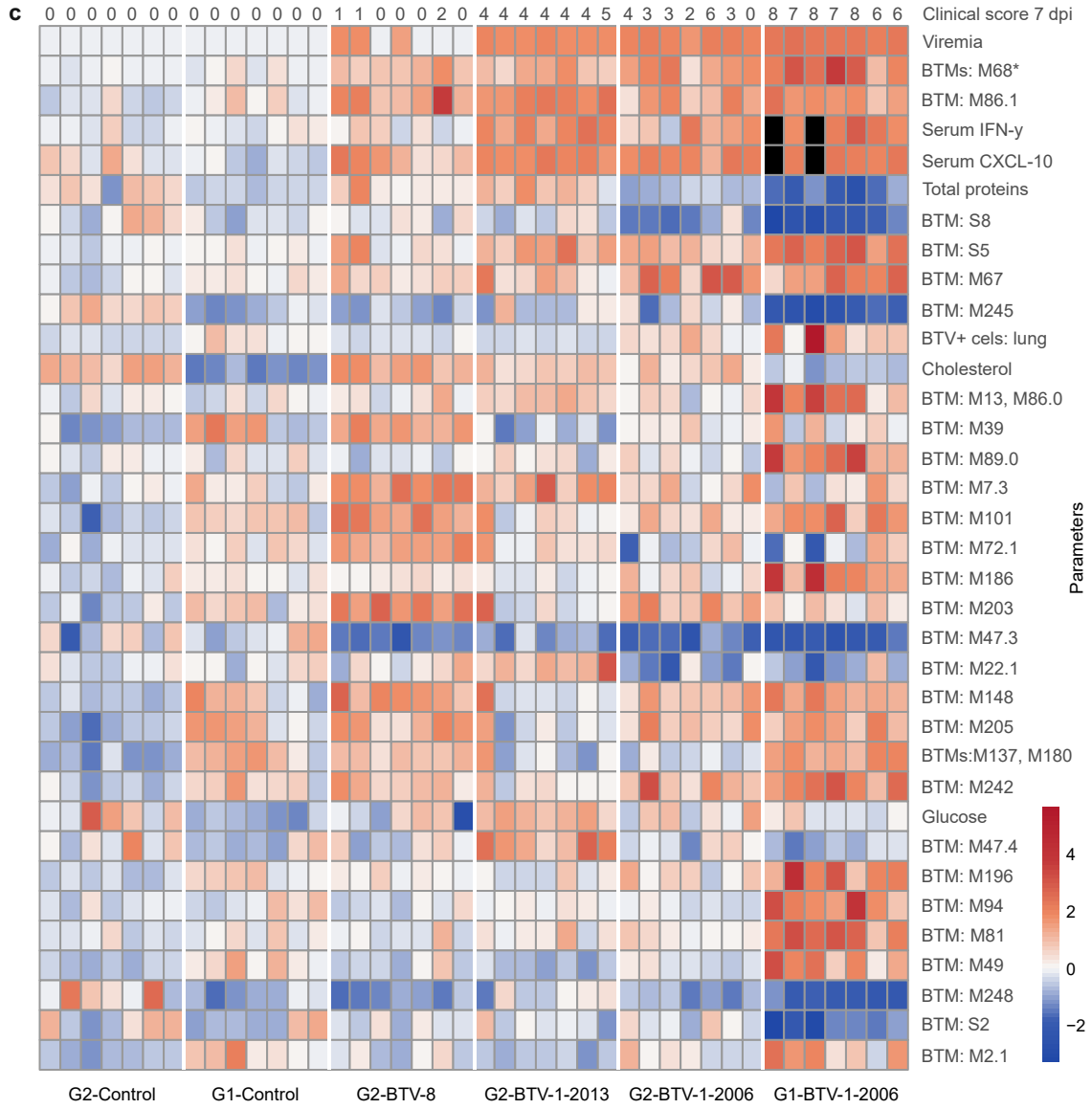

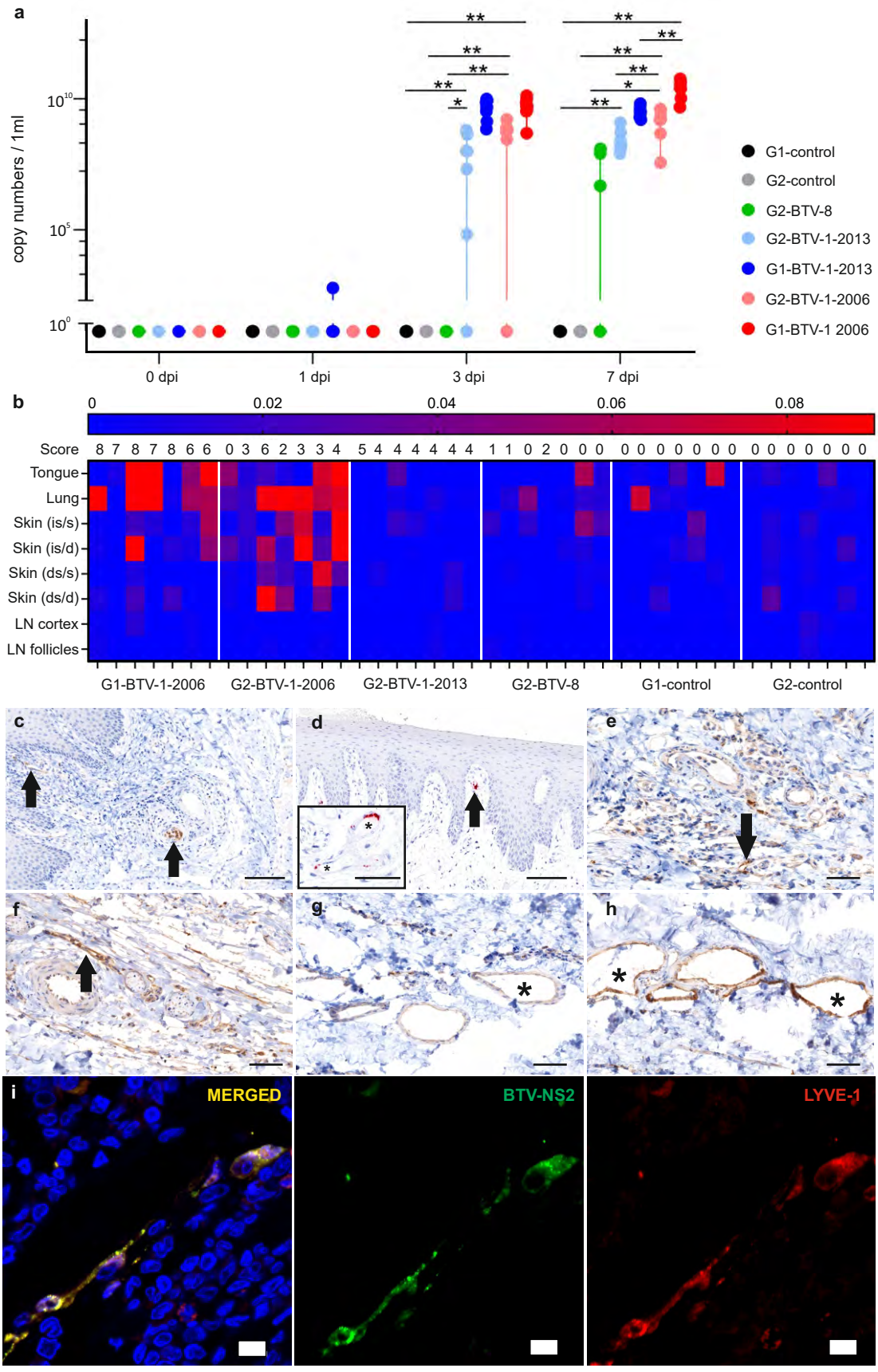

Fig. 4

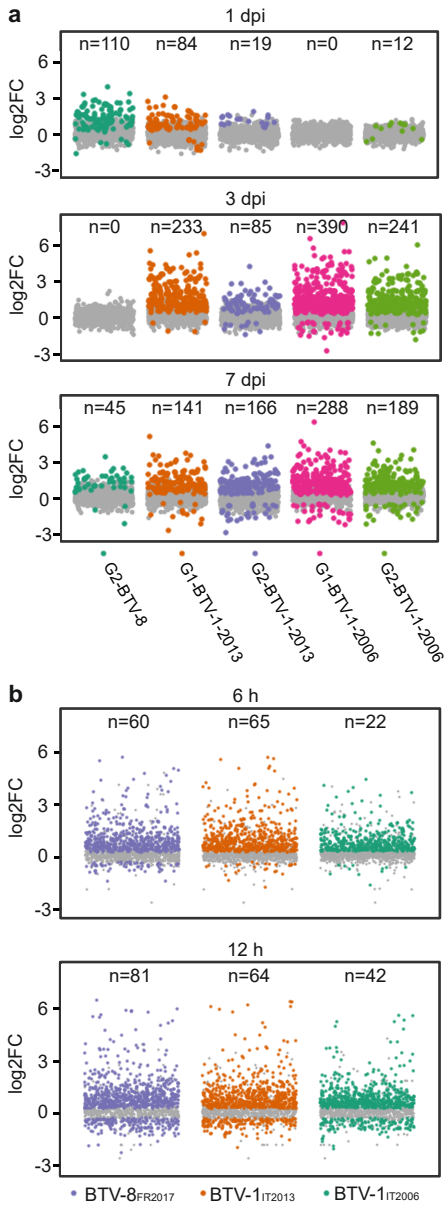

Fig. 5

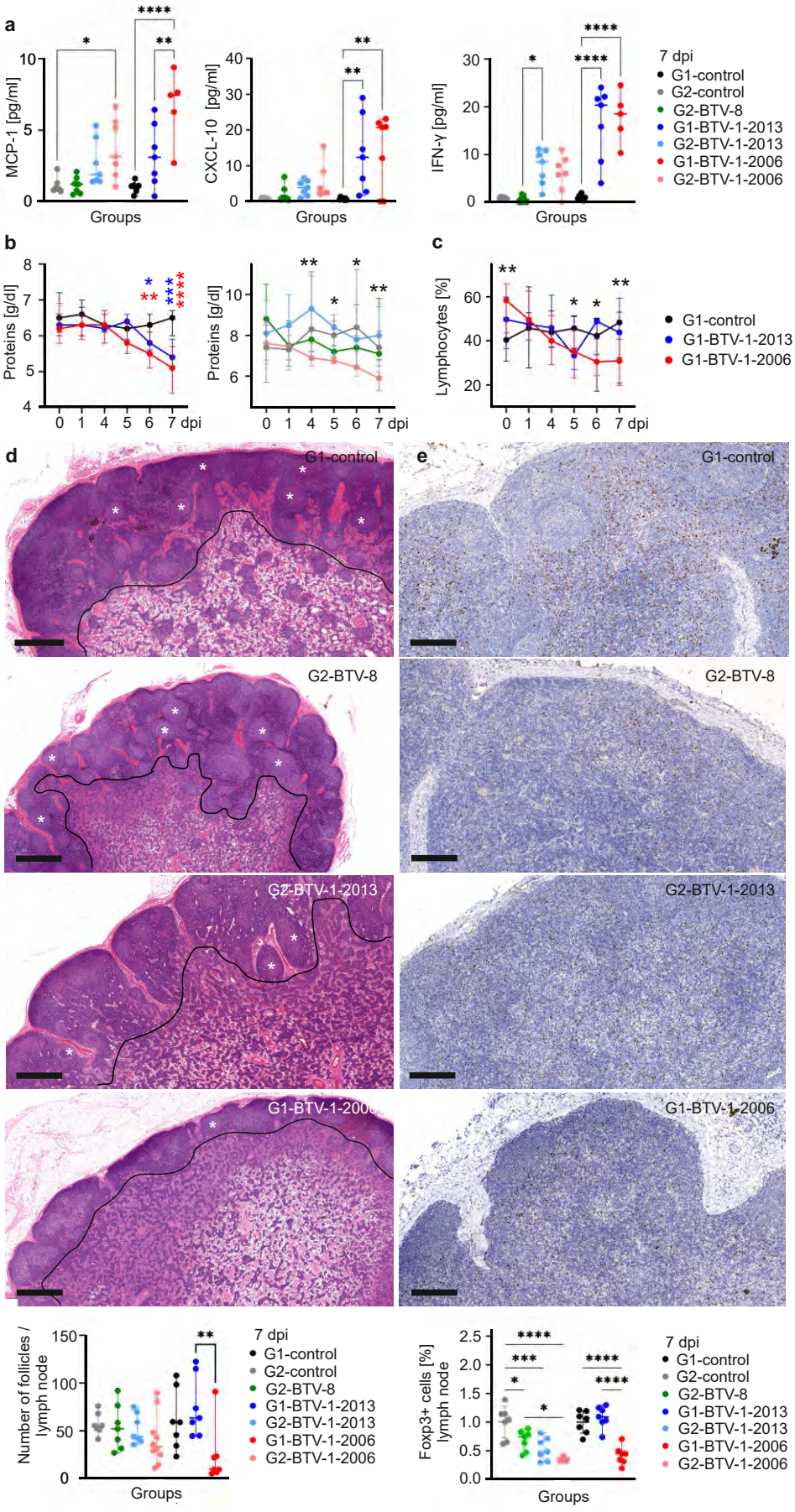

Fig. 6

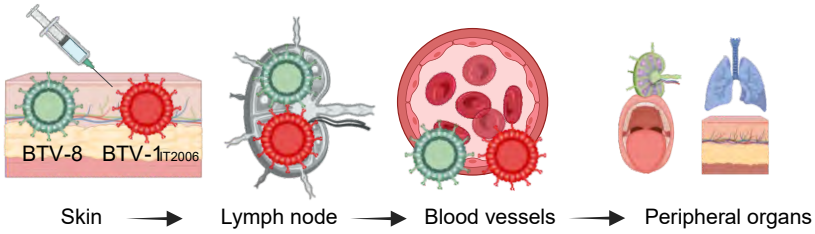

Mild/subclinical outcome

Severe/lethal outcome

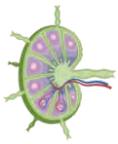

Normal B cell follicles and blood lymphocyte counts

Normal Treg counts

+++	Early ISGs	0
(+)	Late ISGs	+++
(+)	IFNγ	+++
(+)	CXCL-10	+++
(+)	IP-10	+++
(+)	Serum protein loss	+++

Reduced Treg counts

Reduced B cell follicles, lymphopenia

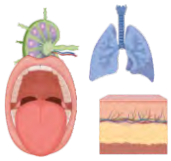

No virus replication in peripheral organs

BTV-8FR2017

Low/ no viraemia

BTV-1IT2006

High viraemia

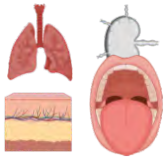

Virus invasion of peipheral organs

BTV-8

Normal temperature

(+)	Oedema, fever	+++
(+)	Respiratory symptoms, ulcerations	+++

Fever

BTV-1IT2006

Fig. 7

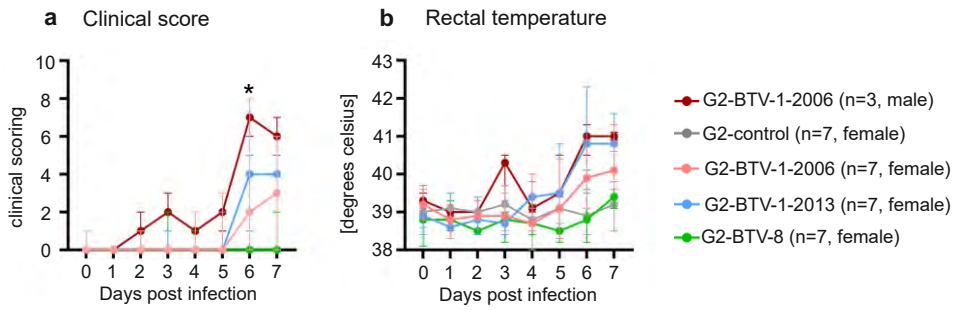

Fig. S1

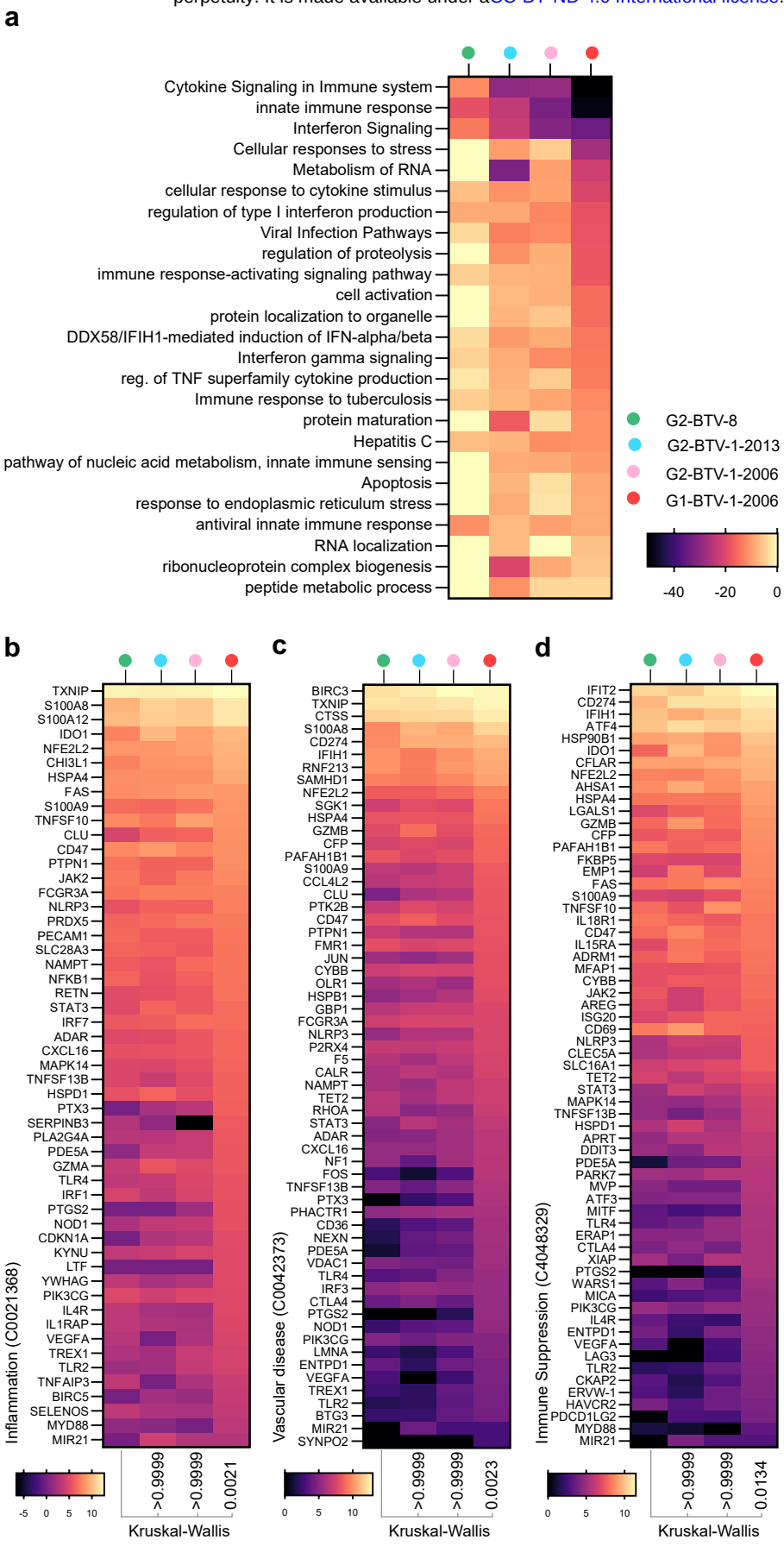

Fig. S2

Table 1. Prediction values for machine learning analysis using “6 states of infection”.

Groups*	G2-control	G2-BTV-1-2013	G2-BTV-1-2006	G2-BTV-8	G1-control	G1-BTV-1-2006
G2-control	999	1	0	0	0	0
G2-BTV-1-2013	39	824	14	123	0	0
G2-BTV-1-2006	0	0	1000	0	0	0
G2-BTV-8	0	0	0	1000	0	0
G1-control	18	0	0	0	982	0
G1-BTV-1-2006	0	0	0	2	0	998

* 1000 repeated random forest cross validations; real states are in the rows and the predictions are the columns.

Table 2. Prediction values for machine learning analysis using “4 states of infection”.

Groups*	G1-/G2-control	G1-/G2-BTV-1-2013	G1-/G2-BTV-1 2006	G1-/G2-BTV-8
G1-/G2-control	987	0	13	0
G1-/G2-BTV-1-2013	0	874	16	110
G1-/G2-BTV-1 2006	80	21	899	0
G1-/G2-BTV-8	26	29	0	945

* 1000 repeated random forest cross validations; real states are in the rows and the predictions are the columns.

Table 3. Prediction values for “clinical states” of infection.

Groups*	Control	Scores 0-2	Scores 3-5	Scores 6-8
Control	851	146	1	2
Scores 0-2	178	479	339	4
Scores 3-5	39	207	694	60
Scores 6-8	129	0	46	825

* 1000 repeated random forest cross validations; real states are in the rows and the predictions are the columns.